

1 **Atmospheric mercury deposition over the land**
2 **surfaces and the associated uncertainties in**
3 **observations and simulations: a critical review**

4 **Lei Zhang^{1,2,*}, Peisheng Zhou¹, Shuzhen Cao¹, and Yu Zhao^{1,2}**

5 ¹ School of the Environment, Nanjing University, 163 Xianlin Avenue, Nanjing,
6 Jiangsu 210023, China

7 ² State Key Laboratory of Pollution Control and Resource Reuse, Nanjing University,
8 163 Xianlin Avenue, Nanjing, Jiangsu 210023, China

9 *Correspondence to:* Lei Zhang (lzhang12@nju.edu.cn)

10 **Abstract.** One of the most important processes in the global mercury (Hg)
11 biogeochemical cycling is the deposition of atmospheric Hg, including gaseous
12 elemental mercury (GEM), gaseous oxidized mercury (GOM), and particulate-bound
13 mercury (PBM), to the land surfaces. Results of wet, dry, and forest Hg deposition
14 from global observation networks, individual monitoring studies, and observation-
15 based simulations have been reviewed in this study. Uncertainties in the observation
16 and simulation of global speciated atmospheric Hg deposition to the land surfaces
17 have been systemically estimated based on assessment of commonly used observation
18 methods, campaign results for comparison of different methods, model evaluation
19 with observation data, and sensitivity analysis for model parameterization. The
20 uncertainties of GOM and PBM dry deposition measurements come from the
21 interference of unwanted Hg forms or incomplete capture of targeted Hg forms, while
22 that of GEM dry deposition observation originates from the lack of standardized
23 experimental system and operating procedure. The large biases in the measurements
24 of GOM and PBM concentration and the high sensitivities of key parameters in
25 resistance models lead to high uncertainties in GOM and PBM dry deposition
26 simulation. Non-precipitation Hg wet deposition could play a crucial role in alpine
27 and coastal regions, and its high uncertainties in both observation and simulation
28 affect the overall uncertainties of Hg wet deposition. The overall uncertainties in the
29 observation and simulation of the total global Hg deposition were estimated to be
30 $\pm(25-50)$ % and $\pm(45-70)$ %, respectively, with the largest contributions from dry

31 deposition. According to the results from uncertainty analysis, future research needs
32 were recommended, among which global Hg dry deposition network, unified methods
33 for GOM and PBM dry deposition measurements, quantitative methods for GOM
34 speciation, campaigns for comprehensive forest Hg behavior, and more efforts on
35 long-term Hg deposition monitoring in Asia are the top priorities.

36

37 **1 Introduction**

38 Mercury (Hg) is a global pollutant, characterized by its neurotoxicity, persistency and
39 bioaccumulation effect. It undergoes regional or global long-range transport via
40 atmospheric circulation, deposition to local or remote areas, methylation in
41 ecosystems, and accumulation through food chain, posing high risks to human health
42 and the environment (Obrist et al., 2018). Hg in the atmosphere has three major
43 forms: gaseous elemental mercury (GEM), gaseous oxidized mercury (GOM), and
44 particulate-bound mercury (PBM). The sum of GEM and GOM is called total gaseous
45 mercury (TGM), and the sum of GOM and PBM is also known as reactive mercury
46 (RM). GEM is the predominant form of atmospheric Hg (>90 %) with a long
47 residence time of several months to over one year due to its chemical inertness and
48 low solubility. GOM used to be estimated to account for less than 1 % of atmospheric
49 Hg, which is easily scavenged by wet deposition, resulting in a short residence time of
50 hours to days (Schroeder and Munthe, 1998; Lindberg et al., 2007). However, recent
51 studies (Lyman et al., 2010; Gustin et al., 2013; McClure et al., 2014; Gustin et al.,
52 2015) showed that there could be a significant underestimation of GOM due to the
53 low capture efficiency of the KCl denuder method adopted by most observation sites
54 in the presence of ozone and moisture. PBM (<10 % of atmospheric Hg) stays in the
55 air for days to several weeks depending on particle size before scavenged by dry or
56 wet deposition (Schroeder and Munthe, 1998; Lindberg et al., 2007; Ci et al., 2012;
57 Fu et al., 2012; Zhang et al., 2016a).

58 Deposition is one of the most important processes in global Hg cycling, leading to
59 the sink of atmospheric Hg (Obrist et al., 2018). According to the Global Mercury
60 Assessment 2018 (UN Environment, 2019), the annual Hg deposition to the land
61 surfaces including freshwater is estimated to be 3600 t. Atmospheric Hg deposition
62 can be broadly divided into wet and dry deposition. Hg wet deposition is mostly in the
63 form of precipitation (rain, snow, etc.), with non-negligible contribution from non-

64 precipitation forms (cloud, fog, dew, frost, etc.). Hg dry deposition is highly related to
65 the underlying surfaces, including forest canopies, grasslands, wetlands, agricultural
66 fields, deserts, background non-vegetated soils, contaminated sites, etc. (Zhang et al.,
67 2009). Forest canopy is regarded as an important sink of atmospheric Hg for its
68 special forms of deposition, litterfall and throughfall (Gustin et al., 2008). Litterfall is
69 a form of indirect Hg dry deposition through foliar uptake of atmospheric Hg, and
70 throughfall includes wet-deposited Hg above the canopy and a portion of dry-
71 deposited Hg washed off from the canopy (Wright et al., 2016). Hg deposition
72 through litterfall has recently been drawn much attention to by the study of Wang et
73 al. (2016a). The sum of litterfall and throughfall is regarded as the total Hg deposition
74 in forest canopies.

75 Significant efforts have been made in the past decade on quantifying atmospheric
76 Hg deposition through both direct observations and model simulations, especially on
77 dry deposition (Lyman et al., 2009; Zhang et al., 2009; Holmes et al., 2011; Lai et al.,
78 2011; Castro et al., 2012; Gustin et al., 2012; Peterson et al., 2012; L. Zhang et al.,
79 2012; Fang et al., 2013; Sather et al., 2013; Lynam et al., 2014; Sather et al., 2014;
80 Huang and Gustin, 2015a; Weiss-Penzias et al., 2016a; Zhang et al., 2016b; Hall et al.,
81 2017; Sprovieri et al., 2017). Yet large uncertainties still exist due to limitations of the
82 current methods for Hg deposition measurements and modeling (Gustin et al., 2015).
83 The purpose of this paper is to give an overview of the uncertainties in the observation
84 and simulation of global speciated atmospheric Hg deposition over the land surfaces.
85 In this paper, we investigated results from observations and simulations of global Hg
86 deposition, reviewed methods adopted for Hg deposition measurements and modeling,
87 estimated the uncertainties of different methods for different Hg deposition forms, and
88 summarized the overall uncertainty level of the global Hg deposition.

89 **2 Observation-based estimation of global Hg deposition**

90 **2.1 Wet deposition**

91 Precipitation is the major form of Hg wet deposition. There have been several
92 observation networks of Hg wet deposition through precipitation. The Global Mercury
93 Observation System (GMOS) is so far the only global scale network covering the
94 northern hemisphere, the tropics, and the southern hemisphere (Sprovieri et al., 2017).
95 The Mercury Deposition Network (MDN) of the National Atmospheric Deposition

96 Program (NADP) in North America is the earliest continental scale network
97 specifically for Hg deposition (Prestbo and Gay, 2009; Weiss-Penzias et al., 2016a).
98 Hg wet deposition is also monitored in the European Monitoring and Evaluation
99 Programme (EMEP) for Europe (Tørseth et al., 2012; Bieser et al., 2014). A new
100 Asia–Pacific Mercury Monitoring Network (APMMN) has recently been established
101 (Sheu et al., 2019).

102 Sprovieri et al. (2017) reported a 5-year record (2011–2015) of Hg wet deposition
103 at 17 selected GMOS monitoring sites, which provided a global baseline of the Hg
104 wet deposition flux including regions in the southern hemisphere and tropical areas.
105 The annual averages (multiple year ranges) of Hg wet deposition in the northern
106 hemisphere, the tropics, and the southern hemisphere were 2.9 (0.2–6.7), 4.7 (2.4–
107 7.0), and 1.9 (0.3–3.3) $\mu\text{g m}^{-2} \text{yr}^{-1}$, respectively. The MDN network has a much
108 longer history dating back to the 1990s. Weiss-Penzias et al. (2016a) analyzed records
109 from 19 sites in the United States (U.S.) and Canada between 1997 and 2013, and
110 discovered trends of Hg concentration in wet deposition, with the early time period
111 (1998–2007) producing a significantly negative trend ($-1.5 \pm 0.2 \%$ yr^{-1}) and the late
112 time period (2008–2013) a flat slope (not significant). Therefore, the MDN data of
113 136 sites for the time period of 2008–2015 (<http://nadp.slh.wisc.edu/mdn>) were used
114 in Figure 1 to represent the recent background Hg wet deposition level in North
115 America. Fu et al. (2016a) summarized wet deposition measurements from 7
116 monitoring sites in China. The annual Hg wet deposition fluxes at 6 rural sites were
117 averagely $4.8 \mu\text{g m}^{-2} \text{yr}^{-1}$, while the annual flux at an urban site was as high as 12.6
118 $\mu\text{g m}^{-2} \text{yr}^{-1}$.

119 Figure 1 summarizes the global distribution of the observed Hg wet deposition
120 fluxes based on results from both these global or regional networks and individual
121 studies. Overall, East Asia has the highest wet deposition flux (averagely $16.1 \mu\text{g m}^{-2}$
122 yr^{-1}), especially in the southern part of China where the RM concentration level is
123 relatively high (Fu et al., 2008; Guo et al., 2008; Wang et al., 2009; Fu et al., 2010a;
124 2010b; Ahn et al., 2011; Huang et al., 2012b; Seo et al., 2012; Huang et al., 2013a;
125 Sheu and Lin, 2013; Marumoto and Matsuyama, 2014; Xu et al., 2014; Zhu et al.,
126 2014; Huang et al., 2015; Zhao et al., 2015; Han et al., 2016; Fu et al., 2016a; Ma et
127 al., 2016; Nguyen et al., 2016; Qin et al., 2016; Sommar et al., 2016; Cheng et al.,
128 2017; Travnikov et al., 2017; Chen et al., 2018; Lu and Liu, 2018). North America has

129 an average Hg wet deposition flux of $9.1 \mu\text{g m}^{-2} \text{yr}^{-1}$, and exhibits a descending
130 spatial profile from the southeastern part to the northwestern part, which is consistent
131 with the distribution of the atmospheric Hg concentration (L. Zhang et al., 2012;
132 Gichuki and Mason, 2014; Lynam et al., 2017). Europe has the lowest Hg wet
133 deposition level (averagely $3.4 \mu\text{g m}^{-2} \text{yr}^{-1}$) according to the available observation and
134 simulation data (Connan et al., 2013; Bieser et al., 2014; Siudek et al., 2016).
135 Observation data for the tropics and the southern hemisphere are scarce with large
136 uncertainties (Wetang'ula, 2011; Gichuki and Manson, 2013; Sprovieri et al., 2017).
137 The one exceptional tropical site with a wet deposition flux of $16.8 \mu\text{g m}^{-2} \text{yr}^{-1}$ is in
138 Kenya while the other sites in the tropics are all in Mexico (Wetang'ula, 2011; Hansen
139 and Gay, 2013). The two sites in the southern hemisphere with annual precipitation of
140 over 4000 mm are in Australia and have wet deposition fluxes of 29.1 and $18.2 \mu\text{g m}^{-2}$
141 yr^{-1} , respectively (Dutt et al., 2009). Seen from the bottom part of Figure 1, Hg wet
142 deposition flux is not significantly correlated with elevation.

143 Studies on non-precipitation Hg wet deposition (e.g., cloud, fog, dew, and frost) are
144 very limited so far. Fog or cloud Hg deposition is not yet considered in the global Hg
145 wet deposition observation network. However, studies (Stankwitz et al., 2012; Weiss-
146 Penzias et al., 2016b; Gerson et al., 2017) have shown that cloud and fog water have
147 higher Hg concentration than rain water in the same region, and cloud and fog could
148 have a remarkable contribution to Hg wet deposition in high-elevation forests and
149 near-water surfaces. Stankwitz et al. (2012) and Gerson et al. (2017) found the
150 average cloud Hg deposition fluxes of two North American montane forests to be 7.4
151 and $4.3 \mu\text{g m}^{-2}$ during the research periods, respectively, equivalent to rainfall Hg
152 deposition. In California coastline, fog Hg deposition, with only 2 % volume
153 proportion, accounts for 13 % of the total wet deposition (Weiss-Penzias et al.,
154 2016b). Converse et al. (2014) found the annual dew and frost Hg deposition at a
155 high-elevation meadow in the U.S. to be about $0.12 \mu\text{g m}^{-2} \text{yr}^{-1}$, 2–3 orders of
156 magnitude smaller than wet deposition through precipitation. More standardized
157 methods are in urgent need for non-precipitation Hg wet deposition measurements.

158 **2.2 Dry deposition**

159 Figure 2 shows the global distribution of the GOM, PBM and GEM dry deposition
160 fluxes from observation-based estimation, either direct observation of dry deposition
161 or simulation based on Hg concentration observation. The global Hg dry deposition

162 network is very immature compared to the wet deposition network due to the
163 inconsistency in methods for estimation. GOM dry deposition fluxes were either
164 measured by the surrogate surface methods or simulated based on GOM concentration
165 measurements. PBM dry deposition fluxes were mainly estimated from the
166 measurements of total or size-resolved PBM concentrations. GEM dry deposition
167 fluxes were measured by different types of methods, including the surrogate surface
168 methods, the enclosure methods, and the micrometeorological methods.

169 Wright et al. (2016) presented an overview of GOM and PBM dry deposition. In
170 their work, the observation or simulation years for nearly one third of the reviewed
171 studies were earlier than 2005, and only studies conducted in North America and Asia
172 were summarized. Therefore, this study included more studies carried out in recent
173 years and limited the observation or simulation year to be no earlier than 2005. Also,
174 studies in Europe and China were summarized in this study. As shown in Figure 2,
175 most studies on GOM dry deposition were conducted in North America and Europe,
176 among which direct observations of GOM dry deposition are mainly from North
177 America (Lyman et al., 2007; Lyman et al., 2009; Weiss-Penzias et al., 2011; Lombard
178 et al., 2011; Castro et al., 2012; Gustin et al., 2012; Peterson et al., 2012; L. Zhang et
179 al., 2012; Sather et al., 2013; Bieser et al., 2014; Sather et al., 2014; Wright et al.,
180 2014; Huang and Guatin, 2015a; Enrico et al., 2016; Han et al., 2016; Zhang et al.,
181 2016b; Huang et al., 2017). Regardless of the estimating methods, the average GOM
182 dry deposition flux in North America ($6.4 \mu\text{g m}^{-2} \text{yr}^{-1}$) is higher than in Europe (3.0
183 $\mu\text{g m}^{-2} \text{yr}^{-1}$). There have been very few studies on GOM dry deposition in Asia. A
184 significant correlation ($R^2=0.532$, $p<0.01$) was found between the elevation and the
185 GOM dry deposition flux (see Figure 3), which could be due to higher GOM
186 concentrations at higher elevation and stronger atmospheric turbulence (Huang and
187 Gustin, 2015a). Nevertheless, significant discrepancies were found between the GOM
188 dry deposition fluxes from direct observations and from model simulations based on
189 measurements of GOM concentrations (see Figure 4). Results from size-resolved
190 PBM analysis and PBM dry deposition models show that East Asia has a much higher
191 average of PBM dry deposition flux ($45.3 \mu\text{g m}^{-2} \text{yr}^{-1}$) than North America ($1.1 \mu\text{g}$
192 $\text{m}^{-2} \text{yr}^{-1}$) (Fang et al., 2012a; Fang et al., 2012b; Zhu et al., 2014; Zhang et al., 2015;
193 Huang et al., 2016; Guo et al., 2017).

194 Zhu et al. (2016) reviewed the air-surface exchange of GEM. The observation years

195 for most of the reviewed studies were earlier than 2005. Since GEM concentrations
196 decreased significantly from early 1990s to 2005 in most regions in the world (Y.
197 Zhang et al., 2016), this study included more recent studies and limited the
198 observation or simulation year to be no earlier than 2005. The average GEM dry
199 deposition is lower in Europe ($4.3 \pm 8.1 \mu\text{g m}^{-2} \text{yr}^{-1}$) while higher in North America
200 with more variation ($5.2 \pm 15.5 \mu\text{g m}^{-2} \text{yr}^{-1}$) (Castelle et al., 2009; Baya and Heyst,
201 2010; Converse et al., 2010; Miller et al., 2011). The four Asian sites using all show
202 negative values, indicating the role of East Asia as a net emission source rather than a
203 net deposition sink (Luo et al., 2016; Ci et al., 2016; Yu et al., 2018). However, the
204 GEM dry deposition observations in Asia are still very limited.

205 Hg dry deposition is highly related to the underlying surfaces. Figure 5 exhibits the
206 dry deposition fluxes of GOM, PBM and GEM for different terrestrial surface types.
207 As shown in Figure 5a, high GOM dry deposition levels were found for grasslands
208 (mainly alpine meadows) and savannas. This is probably because of the enhanced Hg
209 oxidation process at high elevations with more halogen free radicals or more intensive
210 solar radiations (Huang and Gustin, 2015a). Urban areas also have high GOM dry
211 deposition fluxes due to high GOM concentrations. The low GOM dry deposition
212 fluxes on moist surfaces (near-water surfaces and croplands) might be partially
213 because of fog and dew scavenging (Malcolm and Keeler, 2002; Zhang et al., 2009).
214 The PBM dry deposition flux is high on surfaces with high human activities (urban
215 areas and croplands) and low in vegetative areas, implying the heavier PM pollution
216 in urban and rural areas than in remote areas (Figure 5b). Short-term observation of
217 GEM dry deposition shows high fluctuation. Therefore, we summarized model
218 estimations and one annual observation dataset (L. Zhang et al., 2012; Bieser et al.,
219 2014; Zhang et al., 2016b; Enrico et al., 2016), and found that the GEM dry
220 deposition does not only depend on GEM concentration, but also on the air–soil Hg
221 exchange compensation point (Luo et al., 2016). Regarding the annual air–surface Hg
222 exchange, instead of an important natural source, forests tend to be a net sink of
223 atmospheric Hg (Figure 5c).

224 **2.3 Forest deposition**

225 Hg deposition in forests is mainly in the forms of litterfall and throughfall. Wright
226 et al. (2016) also made an extensive review of litterfall and throughfall Hg deposition.
227 Wang et al. (2016a) made a comprehensive assessment of the global Hg deposition

228 through litterfall, and found litterfall Hg deposition an important input to terrestrial
 229 forest ecosystems ($1180 \pm 710 \text{ Mg yr}^{-1}$). Not many new studies on forest Hg deposition
 230 have been reported since then. Therefore, here we only briefly introduce the spatial
 231 distribution of forest Hg deposition. South America was estimated to bear the highest
 232 litterfall Hg deposition ($65.8 \pm 57.5 \mu\text{g m}^{-2} \text{ yr}^{-1}$) around the world (Teixeira et al.,
 233 2012; Buch et al., 2015; Fostier et al., 2015; Teixeira et al., 2017; Fragoso et al., 2018;
 234 Shen et al., 2019). There have been numerous forest Hg deposition studies in the
 235 recent decade in East Asia with the second highest average litterfall Hg deposition
 236 flux ($35.5 \pm 27.7 \mu\text{g m}^{-2} \text{ yr}^{-1}$) (Wan et al., 2009; Wang et al., 2009; Fu et al., 2010a; Fu
 237 et al., 2010b; Gong et al., 2014; Luo et al., 2016; Ma et al., 2015; Han et al., 2016; Fu
 238 et al., 2016a; Ma et al., 2016; Wang et al., 2016b; Zhou et al., 2016; Zhou et al.,
 239 2017). Lower levels of litterfall Hg deposition fluxes were found in North America
 240 ($12.3 \pm 4.9 \mu\text{g m}^{-2} \text{ yr}^{-1}$) and Europe ($14.4 \pm 5.8 \mu\text{g m}^{-2} \text{ yr}^{-1}$) (Larssen et al., 2008; Obrist
 241 et al., 2009; Fisher and Wolfe, 2012; Juillerat et al., 2012; Obrist et al., 2012; Risch et
 242 al., 2012; Benoit et al., 2013; Navrátil et al., 2014; Gerson et al., 2017; Risch et al.,
 243 2017; Risch and Kenski, 2018). Throughfall Hg deposition is another important way
 244 for Hg input in forests, Wright et al. (2016) summarized previous studies and reported
 245 the median throughfall Hg deposition to be 49.0, 16.3 and $7.0 \mu\text{g m}^{-2} \text{ yr}^{-1}$ in Asia,
 246 Europe and North America, respectively. Large discrepancies in Asian co-located
 247 comparisons between rainfall and throughfall Hg depositions (32.9 ± 18.9 and 13.3 ± 8.6
 248 $\mu\text{g m}^{-2} \text{ yr}^{-1}$, respectively) could indicate a high dry deposition level in Asian forests
 249 (Wan et al., 2009; Wang et al., 2009; Fu et al., 2010a; Fu et al., 2010b; Luo et al.,
 250 2016; Ma et al., 2015; Han et al., 2016; Fu et al., 2016a; Ma et al., 2016; Wang et al.,
 251 2016b; Zhou et al., 2016).

252 **3 Uncertainties in Hg deposition observation**

253 **3.1 Uncertainties in the measurements of Hg wet deposition**

254 **3.1.1 Measurements of Hg wet deposition through precipitation**

255 Hg wet deposition through precipitation, mostly rainfall, is easier to measure than dry
 256 deposition and usually more reliable. The rainfall Hg wet deposition flux is calculated
 257 as follows (Zhao et al., 2018):

$$258 \quad F_{\text{wet,rainfall}} = \sum_{i=1}^n C_i \cdot D_i \quad (1)$$

259 where $F_{\text{wet,rainfall}}$ is the total rainfall Hg wet deposition flux; n is the number of
 260 precipitation events during a certain period; C_i is the total Hg concentration in
 261 rainwater during Event i ; and D_i is the precipitation depth of Event i . As shown in Eq.
 262 (1), the overall uncertainty in rainfall Hg wet deposition originates from both the
 263 analytical methods of Hg concentration in rainwater and the measurements of
 264 precipitation depth.

265 Both manual and automatic precipitation sample collectors were used in previous
 266 studies (Fu et al., 2010a; Gratz and Keeler, 2011; Marumoto and Matsuyama, 2014;
 267 Zhu et al., 2014; Brunke et al., 2016; Chen et al., 2018). Automatic precipitation
 268 sample collectors cover the lid automatically when it is not raining to prevent
 269 potential contamination, while manual collectors require manually placing collectors
 270 before precipitation events and retrieving them after events. The measurements of
 271 precipitation volume by samplers have non-negligible uncertainties (Wetherbee,
 272 2017). The relative standard deviations (RSDs) of daily and annual precipitation depth
 273 measurements in MDN were estimated to be 15 % and 10 %, respectively (Wetherbee
 274 et al., 2005). The event-based sampling volume biases of two types of samplers used
 275 in APMMN were estimated to be up to 11–18 % (Sheu et al., 2019).

276 The total Hg concentration in rainwater samples is usually analyzed by oxidation,
 277 purge and trap, and cold vapor atomic fluorescence spectrometry (CVAFS) following
 278 EPA Method 1631. GMOS reported the ongoing precision recovery (OPR) for every
 279 12 samples to be generally within 93–109 % (Sprovieri et al., 2017). The relative
 280 percentage difference (RPD) for MDN precipitation Hg analysis is generally within
 281 10 % according to inter-laboratory comparisons (Wetherbee and Martin, 2018). For
 282 individual studies (Fu et al., 2010a; Huang et al., 2015; Zhao et al., 2018), the RSD is
 283 also generally less than 10 %.

284 The overall relative uncertainty of the precipitation Hg wet deposition flux was
 285 calculated to be approximately $\pm(15\text{--}20)$ % using the following equation:

$$286 \quad \delta_F(\text{wet}) = \frac{U_F(\text{wet})}{F_{\text{wet}}} = \sqrt{\left(\frac{U_C}{C}\right)^2 + \left(\frac{U_D}{D}\right)^2} = \sqrt{\delta_C^2 + \delta_D^2} \quad (2)$$

287 where $\delta_F(\text{wet})$ and $U_F(\text{wet})$ are the relative and absolute uncertainties of Hg wet
 288 deposition flux, respectively; δ_C and U_C are the relative and absolute uncertainties of
 289 the total Hg concentration in precipitation water, respectively; and δ_D and U_D are the
 290 relative and absolute uncertainties of the precipitation depth, respectively.

291 **3.1.2 Measurements of Hg wet deposition through cloud, fog, dew and frost**

292 Non-precipitation Hg wet deposition, e.g., cloud, fog, dew and frost, could account for
293 a notable proportion of the total wet deposition in montane, coastal, arid, and semi-
294 arid areas (Lawson et al., 2003; Sheu and Lin, 2011; Stankwitz et al., 2012; Blackwell
295 and Driscoll, 2015b). Quantifying Hg in cloud or fog helps better understand the
296 impact of long-range transport and local sources on global Hg cycling (Malcolm et al.,
297 2003). The non-precipitation Hg deposition flux is calculated as follows:

$$298 \quad F_{\text{wet, non-precipitation}} = \sum_{j=1}^m C_j \cdot D_j \quad (3)$$

299 where $F_{\text{wet, non-precipitation}}$ is the non-precipitation Hg deposition flux; m is the number
300 of non-precipitation wet deposition events during a certain period; C_j is the total Hg
301 concentration in non-precipitation wet deposition water during Event j ; and D_j is the
302 non-precipitation wet deposition depth of Event j .

303 Both active and passive collectors have been used to collect cloud or fog water
304 (Lawson et al., 2003; Malcolm et al., 2003; Kim et al., 2006; Sheu and Lin, 2011;
305 Schwab et al., 2016; Weiss-Penzias et al., 2018). The major uncertainty lies in the
306 deposition depth. The deposition depth of cloud, fog, dew or frost is usually modeled
307 based on meteorology (Converse et al., 2014; Katata, 2014). The fog deposition depth
308 can be measured by standard fog collectors (SFC). The uncertainty of fog deposition
309 depth measurements is mainly from the collecting efficiency of SFC depending on the
310 wind speed, wind direction, or mesh types (Weiss-Penzias et al., 2016b; Fernandez et
311 al., 2018). Montecinos et al. (2018) evaluated the collection efficiency of SFC to be
312 up to 37 %. Therefore, there is extremely large uncertainty in the measurements of the
313 fog deposition depth. Based on the fog deposition studies (Weiss-Penzias et al.,
314 2016b; Fernandez et al., 2018; Montecinos et al., 2018), the overall uncertainty of
315 non-precipitation Hg deposition flux observation is estimated to be $\pm(200-300)$ %.
316 Note that the true uncertainty range is not symmetric about the mean because some of
317 the underlying variables are lognormally distributed (Streets et al., 2005). A better
318 interpretation of “ $\pm(200-300)$ %” might be “within a factor of 3–4”.

319 **3.2 Uncertainties in the measurements of Hg dry deposition**

320 Direct measurements of the Hg dry deposition flux is technically challenging, large
321 uncertainties still exist in quantify Hg dry deposition accurately (Wright et al., 2016).
322 Three major categories of methods for direct Hg dry deposition measurements are the

323 surrogate surface methods, the enclosure methods, and the micrometeorological
324 methods (Zhang et al., 2009; Huang et al., 2014).

325 **3.2.1 Measurements of RM (GOM and PBM) dry deposition**

326 Most of the RM dry deposition measurements used the surrogate surface methods
327 (Huang et al., 2014; Wright et al., 2016). The micrometeorological methods and the
328 enclosure methods were also adopted in some studies (Poissant et al., 2004; Zhang et
329 al., 2005; Skov et al., 2006), but not widely used due to the high uncertainties in the
330 measurements of GOM and PBM concentrations using the Tekran system. For the
331 surrogate surface methods, the RM dry deposition flux is determined using the
332 following equation (Huang et al., 2014):

$$333 \quad F_{\text{dry,SS}} = \frac{M}{A \cdot t} \quad (4)$$

334 where $F_{\text{dry,SS}}$ is the Hg dry deposition flux using the surrogate surface methods; M
335 is the total Hg amount collected on the material during the sampling period; A is the
336 surface area of the collection material; and t is the exposure time.

337 Different surrogate surfaces were used to measure different RM forms. Mounts
338 with cation-exchange membranes (CEMs) are widely used for GOM dry deposition
339 measurements (Lyman et al., 2007; Lyman et al., 2009; Castro et al., 2012; Huang et
340 al., 2012a; Peterson et al., 2012; Sather et al., 2013). The down-facing aerodynamic
341 mount with CEM is considered to be the most reliable deployment for GOM dry
342 deposition measurements so far (Lyman et al., 2009; Huang et al., 2014). Knife-edge
343 surrogate surface (KSS) samplers with quartz fiber filter (QFFs) and dry deposition
344 plates (DDPs) with overhead projection films were deployed for PBM dry deposition
345 measurements (Lai et al., 2011; Fang et al., 2012b; Fang et al., 2013). However, these
346 samplers are not well verified to reflect the deposition velocity of PBM, and hence not
347 widely accepted. KCl-coated QFFs were used to measure the total RM (GOM+PBM)
348 dry deposition, but failed to capture GOM efficiently (Lyman et al., 2009; Lai et al.,
349 2011).

350 The uncertainties of RM dry deposition mainly come from the capture efficiency of
351 sampling surface, the turbulent condition near the surface, and the analysis of the
352 membrane. CEMs exhibited a GOM capture rate of 51–107 % in an active sampling
353 system (Huang and Gustin, 2015b). The CEM mounts designed to measure only
354 GOM dry deposition capture part of fine PBM (Lyman et al., 2009; Huang et al.,

355 2014), while the KSS samplers with QFFs designed to measure only PBM dry
356 deposition may also collect part of GOM (Rutter and Schauer, 2007; Gustin et al.,
357 2015). Based on the RM concentration measurements and the surrogate surface
358 method evaluations, the GOM concentration related uncertainty is estimated to be
359 $\pm 50\%$ (Lyman et al., 2009; Lyman et al., 2010; Gustin et al., 2012; Fang et al., 2013;
360 Zhang et al., 2013; Huang et al., 2014). The design of the sampler (e.g., the sampler
361 orientation, the shape of the sampler, variation in turbulence, low surface resistances,
362 passivation, etc.) leads to the surface capture efficiency related uncertainty which is
363 about $\pm 50\%$ for GOM (Lyman et al., 2009; Lai et al., 2011; Huang et al., 2012a). The
364 overall uncertainty in surface capture efficiency could decline to about $\pm 30\%$ at
365 annual level. Calculating based on the method described by Eq. (2), the overall
366 uncertainty of GOM dry deposition observation is $\pm(60-70)\%$. There is not enough
367 information to quantify the overall uncertainty of PBM dry deposition observation in
368 a similar way. However, its uncertainty is usually considered to be higher than that of
369 GOM dry deposition measurements. Based on the distribution of daily samples in the
370 study of Fang et al. (2012b), the overall uncertainty of PBM dry deposition
371 measurements is assumed to be $\pm(80-100)\%$.

372 **3.2.2 Measurements of GEM dry deposition**

373 GEM has a low dry deposition velocity due to its mild activity, high volatility and low
374 water solubility, and deposited GEM could re-emit into the atmosphere (Bullock et al.,
375 2008; Fu et al., 2016b). Various methods have been applied to studies on air-surface
376 GEM exchange, among which the enclosure methods and the micrometeorological
377 methods were most commonly used (Zhang et al., 2009; Agnan et al., 2016; Zhu et al.,
378 2016; Yu et al., 2018). Both Agnan et al. (2016) and Zhu et al. (2016) have presented
379 comprehensive reviews on air-surface GEM exchange and introduced the two types
380 of methods for measurements. The uncertainty of air-surface GEM exchange flux
381 using the micrometeorological methods were estimated to be up to $\pm 30\%$ (Meyers et
382 al., 1996; Lindberg and Meyers, 2001; Fritsche et al., 2008; Sommer et al., 2013a;
383 Zhu et al., 2015b). However, Zhu et al. (2016) summarized existing air-surface GEM
384 exchange studies and found that the mean flux using micrometeorological methods is
385 higher than using DFCs by a factor of 2. Agnan et al. (2016) found the uncertainty of
386 GEM flux to be in the range of -180% to $+120\%$. Therefore, the overall uncertainty
387 of GEM dry deposition observation is estimated to be $\pm(100-200)\%$.

388 3.3 Uncertainties in the measurements of Hg deposition in forests

389 In forest ecosystems, the presence of canopy changes the form of Hg deposition. The
390 sum of litterfall and throughfall is more commonly used to represent the total Hg
391 deposition in forests (Wang et al., 2016a; Wright et al., 2016).

392 3.3.1 Litterfall Hg deposition measurements

393 Litterfall Hg deposition includes the dry and wet deposited Hg on leaves and bark as
394 well as the captured Hg emitted from the soil (Blackwell and Driscoll, 2015a; Wright
395 et al., 2016). Litterfall Hg deposition flux is calculated as follows (Fisher and Wolfe,
396 2012):

$$397 \quad F_{\text{litterfall}} = \frac{E_A \cdot C_l \cdot M_l}{A \cdot t} \quad (5)$$

398 where $F_{\text{litterfall}}$ is the litterfall Hg deposition flux; E_A is the litterfall trap area
399 expansion factor (note: leaves outside the area above the trap could fall into the trap
400 due to horizontal air fluctuation); C_l is the Hg mass concentration in litterfall; M_l is the
401 total dry weight of litterfall; A is the litterfall trap area; and t is the sampling time.

402 Litterfall samples are collected during the leaf-growing or -falling seasons with
403 litterfall traps or collectors (Fisher and Wolfe, 2012). Total litterfall consists of leaves
404 and needles, woody material such as twigs and bark, and reproductive bodies such as
405 flowers, seeds, fruits, and nuts (Meier et al., 2006; Risch et al., 2012). The total litter
406 mass collected by different samplers could cause a RSD of 16 % (Risch et al., 2012
407 and Risch et al., 2017). The Hg content in litterfall can be determined by thermal
408 decomposition, amalgamation, and cold vapor atomic absorption spectrophotometry
409 (CVAAS) following EPA Method 7473 (Richardson and Friedland, 2015; Fu et al.,
410 2016a; Zhou et al., 2017; Risch et al., 2017). Alternatively, the litterfall samples can
411 be digested and analyzed following EPA Method 1631E (Fu et al., 2010a; Fisher and
412 Wolfe, 2012). The uncertainty in litterfall Hg content analysis is about ± 7 %
413 according to the Litterfall Mercury Monitoring Network developed by NADP (Risch
414 et al., 2017) and individual studies (Benoit et al., 2013; Ma et al., 2015; Zhou et al.,
415 2016; Gerson et al., 2017).

416 Therefore, the event-based uncertainty of litterfall Hg deposition observation is
417 estimated to be ± 18 % based on Eq. (2). The Litterfall Mercury Monitoring Network
418 and many other studies only collect litterfall during the falling season each year,
419 which will cause some underestimation. Moreover, based on the assumption that the

420 total Hg concentration in litterfall is linearly accumulated during the growing season,
421 some studies estimated litterfall Hg concentration by multiplying a scale factor, which
422 may cause extra uncertainty (Bushey et al., 2008; Poissant et al., 2008; Fu et al.,
423 2010a; Gong et al., 2014). Taking this into consideration, the overall uncertainty of
424 litterfall Hg deposition observation is estimated to be $\pm(20-30)$ %.

425 **3.3.2 Throughfall Hg deposition measurements**

426 Throughfall Hg deposition includes the wet-deposited Hg passing through the canopy
427 and a portion of dry-deposited Hg washed off from the canopy (Blackwell and
428 Driscoll, 2015a; Wright et al., 2016). Throughfall Hg deposition flux is calculated as
429 follows (Fisher and Wolfe, 2012):

$$430 \quad F_{\text{throughfall}} = \frac{E_A \cdot C_t \cdot V_t}{A \cdot t} \quad (6)$$

431 where $F_{\text{throughfall}}$ is the throughfall Hg deposition flux; E_A is the throughfall funnel
432 area expansion factor; C_t is the Hg mass concentration in throughfall; V_t is the total
433 volume of throughfall; A is the throughfall funnel area; and t is the sampling time.

434 Throughfall under canopy is usually collected using a passive bulk throughfall
435 collector with a funnel connected a bottle for water storage (Wang et al., 2009; Fisher
436 and Wolfe, 2012; Åkerblom et al., 2015) or collected as open-field rain collection if
437 the environmental condition permits (Choi et al., 2008; Fu et al., 2010a; Fu et al.,
438 2010b; Han et al., 2016). Attention should be paid to potential litterfall contamination
439 and cloud or fog deposition influence at high elevation sites if the collector is not
440 sheathed (Fisher and Wolfe, 2012; Wright et al., 2016). Throughfall samples are
441 usually analyzed following EPA Method 1631E (Fisher and Wolfe, 2012). Therefore,
442 throughfall Hg deposition should have a similar uncertainty as rainfall Hg deposition.
443 Considering the possible interference for throughfall sample collection, the overall
444 uncertainty of throughfall Hg deposition observation is estimated as $\pm(20-30)$ %.

445 **4 Uncertainties in Hg deposition simulation**

446 **4.1 Uncertainties in models for Hg wet deposition**

447 **4.1.1 Model for precipitation Hg wet deposition**

448 Hg wet deposition through precipitation is an important process in global or regional
449 chemical transport models (CTMs), such as GEOS-Chem and CMAQ-Hg (Lin et al.,
450 2010; Y. Zhang et al., 2012; Bieser et al., 2014; J. Zhu et al., 2015; Horowitz et al.,

451 2017). As shown in Eq. (1), precipitation Hg wet deposition is the product of the total
452 Hg concentration in rainwater and the precipitation depth. In CTMs, the precipitation
453 Hg concentration contains more uncertain factors. Hg in rainwater originates from the
454 scavenging of GOM and PBM in both free troposphere and boundary layer. Based on
455 previous modeling work for Hg wet deposition in the United States using GEOS-
456 Chem (Selin and Jacob, 2008), GOM and PBM contributed 89 % and 11 % to the total
457 Hg wet deposition, respectively, and 60% of the GOM induced wet deposition
458 originated from scavenging in the free troposphere. Seo et al. (2012) and Cheng et al.
459 (2015) also reported higher scavenging coefficient for GOM than for PBM. Therefore,
460 Hg redox chemistry in the free troposphere, aqueous phase Hg speciation, aqueous
461 phase sorption, and the scavenging process tend to be the dominant sources of
462 uncertainties (Lin et al., 2006; Lin et al., 2007; Cheng et al., 2015).

463 In the simulation of Hg wet deposition by the GEOS-Chem model, the uncertainty
464 of precipitation depth is usually within ± 10 % because it is based on assimilated
465 meteorological observations from the Goddard Earth Observing System (GEOS)
466 instead of meteorological models (Y. Zhang et al., 2012). Y. Zhang et al. (2012)
467 conducted a nested-grid simulation of Hg over North America using GEOS-Chem,
468 and reported the normalized bias of the annual Hg wet deposition flux to be ranging
469 from -14 % to $+27$ % comparing to the MDN observations. Horowitz et al. (2017)
470 used GEOS-Chem to reproduce observed Hg wet deposition fluxes over North
471 America, Europe, and China and also got low bias (0–30 %). The CMAQ-Hg model
472 exhibits a higher uncertainty level because the precipitation depth is simulated by
473 meteorological models (e.g., MM5 or WRF) and its uncertainty has a strong impact
474 on model prediction on Hg wet deposition (Lin et al., 2006). In the study of Bullock et
475 al. (2009), the precipitation simulated by MM5 was averagely 12% greater than
476 observed and the CMAQ simulation of Hg wet deposition was averagely about 15%
477 above the MDN observations. However, different boundary conditions could cause a
478 25% difference (Bullock et al., 2009). Holloway et al. (2012) found that the CMAQ-
479 Hg model underestimated wet deposition by 21 % on an annual basis and showed
480 average errors of 55 %. Based on the comparison between observed and modeled
481 results and the sensitivity of key parameters, the overall uncertainty of precipitation
482 Hg wet deposition simulation is estimated to be $\pm(30-50)$ % depending on the adopted
483 models.

484 **4.1.2 Model for non-precipitation Hg wet deposition**

485 Non-precipitation Hg wet deposition simulation has never been considered in CTMs,
486 but performed in some individual studies with Hg concentration data for cloud, fog,
487 dew or frost samples (Ritchie et al., 2006; Converse et al., 2014; Blackwell and
488 Driscoll, 2015b). Non-precipitation deposition depth can be estimated using resistance
489 models, analytical models or sophisticated atmosphere-soil-vegetation models. Katata
490 (2014) reviewed different types of models for fog deposition estimation, and found
491 the four most sensitive factors to be canopy homogeneity, droplet size spectra, droplet
492 capture efficiency, and canopy structure. Since fog is the most important form of non-
493 precipitation deposition, the overall uncertainty in the simulation of non-precipitation
494 Hg wet deposition is estimated to be $\pm(200\text{--}300)$ % or a factor of 3–4 based on the
495 sensitivity analysis in the study of Katata (2014).

496 **4.2 Uncertainties in models for Hg dry deposition**

497 Hg dry deposition flux is proportional to the corresponding Hg concentration (Zhang
498 et al., 2009):

$$499 \quad F_{\text{dry}} = v_d \cdot C_z \quad (7)$$

500 where F_{dry} is the Hg dry deposition flux; C_z is the Hg concentration at reference
501 height z ; and v_d is the dry deposition velocity.

502 In this part, the uncertainties of speciated Hg concentration measurements were
503 first discussed, followed by the uncertainty analyses of Hg dry deposition models.

504 **4.2.1 Uncertainties in speciated Hg concentration measurements**

505 Although many new methods and apparatus have been or are being developed to
506 better determine speciated Hg concentrations in ambient air, up to now the Tekran
507 2537/1130/1135 system is still the most widely used commercial instrument for
508 continuous measurements of speciated Hg (Gustin et al., 2015). Regional and global
509 monitoring networks such as Atmospheric Mercury Network (AMNet) and GMOS
510 have all been using the Tekran systems and developed systematic quality assurance
511 and quality control (QA/QC) protocols to assure data quality (Obrist et al., 2018).
512 Therefore, this section is mainly to assess the uncertainties of the Tekran system.

513 Tekran 2537 uses a pair of gold trap cartridges (A/B) to capture GEM in order to
514 achieve continuous observation and to reduce the uncertainty of GEM measurements.
515 The standard operating procedure (SOP) of GMOS for the determination of GEM

516 requires the RPD of the average of five consecutive A trap concentrations and five
517 consecutive B trap concentrations to be less than 10 % (Sprovieri et al., 2017). In field
518 comparisons held by EMEP, the RSD from Tekran measurements are also generally
519 within 10 % (Aas, 2006). However, in the Reno Atmospheric Mercury
520 Intercomparison eXperiment (RAMIX) campaign, the RPD between two co-located
521 Tekran systems was as high as 25–35 % (Gustin et al., 2013). This was possibly
522 related to other factors, such as the configuration of the manifold, which could be
523 occasional or systemic. Therefore, the overall uncertainty of GEM concentration
524 measurements by the Tekran system is estimated to be $\pm(10-30)$ %.

525 Tekran 1130 uses a KCl-coated denuder to pre-concentrate GOM, and the collected
526 GOM is then thermally desorbed at 500 °C and converted to GEM for quantification.
527 A number of studies have reported the significant interference of ozone and humidity
528 on the GOM capture rate of the denuder (Lyman et al., 2010; Jaffe et al., 2014;
529 McClure et al., 2014; Gustin et al., 2015). McClure et al., (2014) found that the KCl-
530 coated denuder only captures 20–54 % HgBr_2 in the ambient air under the influence
531 of humidity and ozone. Huang et al. (2013) compared denuder- and membrane-based
532 methods, and reported that the KCl-coated denuder only captures 27–60 % of the
533 GOM measured by CEMs. Discrepancy with a factor of 2–3 at times was found
534 between the Tekran system and other new methods in the RAMIX campaign (Gustin
535 et al., 2013). Cheng and Zhang (2017) developed a numerical method to assess the
536 uncertainty of GOM measurements, and estimated the GOM concentrations measured
537 at 13 AMNet sites to be underestimated by a factor of 1.3 to more than 2. Gustin et al.
538 (2015) reported that the capture efficiency ratio of CEMs over the denuder method for
539 five major GOM compounds ranges from 1.6 to 12.6. Recent studies (Huang and
540 Gustin, 2015a; Huang et al., 2017) applied a correction factor of 3 for Tekran GOM
541 data when modeling dry deposition flux. Therefore, the overall uncertainty of the
542 GOM concentration measured by the Tekran system is estimated to be ± 200 % or
543 within a factor of 3. It should be noted that the correction factor of 3 is not universally
544 applicable. Different humidity levels or ozone concentrations lead to a significant
545 change in underestimation. Different chemical forms of GOM also have different KCl
546 capture efficiencies. Therefore, accurate quantification methods for measuring the
547 total and chemically speciated GOM concentration are in urgent needs.

548 Tekran 1135 uses a quartz filter downstream the KCl denuder to collect $\text{PM}_{2.5}$, and
549 the collected fine particles are then thermally desorbed at 800 °C at a pyrolyzer and

550 converted to GEM for the quantification of PBM, or rather PBM_{2.5}. The uncertainties
 551 in PBM concentration measurements have not been systemically assessed so far.
 552 Gustin et al. (2015) pointed out that breakthrough of GOM from the upstream denuder
 553 could result in the retention of GOM on the quartz filter and induce consequent PBM
 554 overestimation. The RAMIX campaign showed that the RSD of PBM measurements
 555 was 70–100 % when the Tekran systems were free standing (Gustin et al., 2013).
 556 Coarse PBM is neglected in Tekran measurements with an impactor removing all
 557 coarse particles. However, based on the estimation of Zhang et al. (2016b), about
 558 30 % of PBM could be on coarse particles. Regarding the limited evidence from
 559 previous studies, the overall uncertainty of the PBM concentration measured by the
 560 Tekran system is estimated to be ±100 % or a factor of 2.

561 4.2.2 Resistance model for GOM dry deposition

562 Based on Eq. (7), the dry deposition velocity (v_d) is the key parameter in the
 563 determination of Hg dry deposition flux. It can be estimated using a resistance model
 564 (Zhang et al., 2002; Zhang et al., 2003):

$$565 \quad v_d = \frac{1}{R_a + R_b + R_c} \quad (8)$$

566 where R_a is the aerodynamic resistance depending on the meteorological conditions
 567 and the land use category; R_b is the quasi-laminar resistance, a function of friction
 568 velocity and the molecular diffusivity of each chemical species (Zhang et al., 2002);
 569 and R_c is the canopy resistance which can be further parameterized as follows:

$$570 \quad R_c = \left(\frac{1 - W_{st}}{R_{st} + R_m} + \frac{1}{R_{ns}} \right)^{-1} \quad (9)$$

571 where W_{st} is the fraction of stomatal blocking under wet conditions; R_{st} is the
 572 stomatal resistance; R_m is the mesophyll resistance; and R_{ns} is the non-stomatal
 573 resistance which is comprised of in-canopy, soil, and cuticle resistances. Cuticle and
 574 soil resistances for GOM are scaled to those of SO₂ and O₃ by the following equation:

$$575 \quad R_{x,GOM} = \left(\frac{\alpha_{GOM}}{R_{x,SO_2}} + \frac{\beta_{GOM}}{R_{x,O_3}} \right)^{-1} \quad (10)$$

576 where R_x is the cuticle or soil resistance; α and β are two scaling parameters (Zhang
 577 et al., 2003; L. Zhang et al., 2012). Among the numerous parameters in the resistance
 578 model the two scaling factors for the non-stomatal resistance components regarding
 579 the solubility and reactivity of the chemical species are the most sensitive ones. The

580 values for HNO_3 ($\alpha=\beta=10$) used to be applied in the model for GOM (Marsik et al.,
581 2007; Castro et al., 2012; L. Zhang et al., 2012). However, some other studies found
582 the values for HONO ($\alpha=\beta=2$) are probably more suitable for GOM due to equivalent
583 effective Henry's Law constants (H^*) between HONO and HgCl_2 (Lyman et al.,
584 2007). Huang and Gustin (2015a) indicated that no single value could be used to
585 calculate GOM dry deposition due to the unknown GOM compounds. Various values
586 for the two scaling parameters ($\alpha=\beta=2, 5, 7$ and 10) were used in Huang et al. (2017)
587 to identify dominant GOM deposition species.

588 The uncertainties of R_a and R_b are estimated to be generally small, within the range
589 of $\pm 30\%$ (Zhang et al., 2003; Huang et al., 2012a), while the uncertainty of R_c usually
590 has a larger impact, especially through the selection of α and β . Lyman et al. (2007)
591 changed the values of α and β from 2 to 10, and found a 120% enhancement of v_d .
592 With a correction factor of 3 for the GOM concentration measured by Tekran, Huang
593 and Gustin (2015a) got similar modeled and measured GOM dry deposition values
594 with bias of up to $\pm 100\%$. Huang et al. (2017) also applied the correction factor of 3,
595 tested different values of α and β , and found the bias of GOM dry deposition
596 simulation to be up to a factor of 2.5. As discussed above, the overall uncertainty of
597 the GOM concentration measured by Tekran is within a factor of 3. If the GOM dry
598 deposition simulation is directly based on the Tekran GOM data, its uncertainty level
599 would be much higher than a factor of 3. However, recent studies (Huang et al., 2014;
600 Huang and Gustin, 2015a; Huang et al., 2017) have used a correction factor of 3 for
601 GOM concentration data which offsets the uncertainty of GOM dry deposition.
602 Therefore, the overall uncertainty in GOM dry deposition simulation is estimated to
603 be a factor of 2.5–4 or $\pm(150\text{--}300)\%$.

604 **4.2.3 Resistance model for PBM dry deposition**

605 For PBM dry deposition, resistance models regarding both fine and coarse particles
606 are more and more widely applied based on the theory that v_d for atmospheric
607 particles strongly depends on particle size (Dastoor and Larocque, 2004; Zhang et al.,
608 2009; Zhang and He, 2014). Many independent studies (Fang et al., 2012b; Zhu et al.,
609 2014) showed that Hg in coarse particles constitutes a large mass fraction of the total
610 PBM, which was previously neglected. PBM measured by Tekran 2537/1130/1135
611 only considers fine particles. Taking coarse particles into consideration, the total PBM
612 dry deposition is calculated as follows (Zhang et al., 2016b):

613
$$F_{\text{dry,PBM}} = C_f \left(v_f + \frac{f}{1-f} v_c \right) \quad (11)$$

614 where $F_{\text{dry,PBM}}$ is the total PBM dry deposition flux; C_f is the mass concentration of
 615 PBM in fine particles; v_f and v_c are the dry deposition velocities of PBM for fine and
 616 coarse particles, respectively; and f is the mass fraction of PBM in coarse particles. v_f
 617 and v_c can be calculated using the following equation (Zhang et al., 2001):

618
$$v_x = v_g + \frac{1}{R_a + R_s} \quad (12)$$

619 where v_x is v_f or v_c ; v_g is the gravitational settling velocity; R_a is the aerodynamic
 620 resistance; and R_s is the surface resistance which can be parameterized as a function of
 621 collection efficiencies from Brownian diffusion, impaction, and interception
 622 mechanisms (L. Zhang et al., 2012; Zhang et al., 2016b). Zhang and He (2014) have
 623 developed an easier bulk algorithm based on the v_x scheme of Zhang et al. (2001) to
 624 make this model more widely applicable in monitoring networks.

625 Zhang et al. (2001) conducted a model comparison with two PBM dry deposition
 626 schemes, and the results showed that the differences between models are generally
 627 within the range of 20 %. However, recent studies found the proportion of coarse
 628 particles plays a crucial role in the evaluation of PBM dry deposition velocity (Zhang
 629 et al., 2016b). Zhang et al. (2016b) assumed that 30 % of the total PBM is on coarse
 630 particles, and found that 44 % PBM deposition was caused by coarse particle
 631 deposition. We tested the model used by Zhang et al. (2016b), and found a 2-fold
 632 change when we increased the coarse PBM proportion from 30 % to 50%. In other
 633 words, the uncertainty of the PBM deposition velocity could be about $\pm(60-100)$ %.
 634 As discussed above, the overall uncertainty of the PBM concentration measured by
 635 Tekran is about ± 100 %. Considering both aspects and applying the calculation
 636 method based on Eq. (2), the overall PBM uncertainty in GOM dry deposition
 637 simulation is estimated to be $\pm(120-150)$ %.

638 **4.2.4 Bidirectional model for GEM dry deposition**

639 GEM dry deposition can also be calculated using the resistance model with different
 640 parameters. However, the re-emission and natural emission of GEM must be taken
 641 into consideration. Net GEM dry deposition is estimated from the difference between
 642 the estimated unidirectional deposition flux and the modeled total re-emission plus
 643 natural emission in the resistance model (L. Zhang et al., 2012).

644 A bidirectional air-surface exchange model modified from the resistance model is
 645 more and more recommended in recent years (Zhang et al., 2009; Bash, 2010; Wang
 646 et al., 2014; Zhang et al., 2016b; Zhu et al., 2016). In the bidirectional scheme, the
 647 GEM dry deposition flux can be calculated as follows (Zhang et al., 2009):

$$648 \quad F_{\text{dry,GEM}} = \frac{\chi_a - \chi_c}{R_a + R_b} \quad (13)$$

$$649 \quad \chi_c = \left(\frac{\chi_a}{R_a + R_b} + \frac{\chi_{st}}{R_{st} + R_m} + \frac{\chi_g}{R_{ac} + R_g} \right) \left(\frac{1}{R_a + R_b} + \frac{1}{R_{st} + R_m} + \frac{1}{R_{ac} + R_g} + \frac{1}{R_{cut}} \right)^{-1} \quad (14)$$

650 where $F_{\text{dry,GEM}}$ is the net GEM dry deposition flux; χ_a is the GEM concentration at a
 651 reference height; R_a , R_b , R_{st} , R_m , R_{ac} , R_g and R_{cut} are aerodynamic, quasi-laminar,
 652 stomatal, mesophyll, in-canopy aerodynamic, ground surface and cuticle resistances,
 653 respectively (Zhang et al., 2016b); and χ_{st} and χ_g are canopy, stomatal and ground
 654 surface compensation points, respectively. Based on observations on different land use
 655 categories, Wright and Zhang (2015) have proposed a range of χ_{st} and χ_g .

656 The studies of L. Zhang et al. (2012) and Zhang et al. (2016b) have shown the great
 657 importance of the previously neglected GEM dry deposition. Due to the presence of
 658 natural and re-emission of GEM, the net GEM dry deposition has a higher uncertainty
 659 level than GOM and PBM dry deposition. Although both the studies of L. Zhang et al.
 660 (2012) and Zhang et al. (2016b) reported the uncertainty of net GEM dry deposition to
 661 be averagely about a factor of 2, there were many exceptions (over a factor of 2–5)
 662 according to L. Zhang et al. (2012), especially when the net GEM dry deposition
 663 fluxes were at low level. Based on the above concern and the sensitivity analysis
 664 conducted in the study of Zhang et al. (2016b), the overall uncertainty of the net GEM
 665 dry deposition simulation is within a factor of 2 or $\pm 100\%$ when GEM dominates the
 666 total Hg dry deposition, while it could be as high as a factor of 5 or $\pm 400\%$ when
 667 GOM+PBM dominate the total dry deposition.

668 4.3 Uncertainties in models for forest Hg deposition

669 The study of Wang et al. (2016a) is to date the only modeling study for litterfall Hg
 670 deposition. Monte Carlo simulation was adopted to assess the global Hg deposition
 671 through litterfall based on the measured litterfall Hg concentrations and the global
 672 litterfall biomass distribution. The estimated global annual Hg deposition through
 673 litterfall was reported to be 1180 t with a relative uncertainty of $\pm 60\%$. At the site
 674 level comparison, the difference is within a factor of 2. Therefore, the overall

675 uncertainty of litterfall Hg deposition is estimated to be $\pm(60-100)$ %. There is no
 676 modeling study on throughfall Hg deposition so far. Consequently, we can only use
 677 the overall uncertainty of wet and dry deposition simulation to represent throughfall,
 678 which will be discussed in the next section.

679 **5 Summary of uncertainties in Hg deposition to terrestrial surfaces**

680 Based on the review work above, the overall uncertainties of wet, dry, and forest Hg
 681 deposition can be calculated using the following equation:

$$682 \quad \delta_{A+B} = \frac{U_{A+B}}{F_{A+B}} = \frac{\sqrt{U_A^2 + U_B^2}}{F_{A+B}} = \frac{\sqrt{F_{A+B}^2 P_A^2 \delta_A^2 + F_{A+B}^2 P_B^2 \delta_B^2}}{F_{A+B}} = \sqrt{P_A^2 \delta_A^2 + P_B^2 \delta_B^2} \quad (15)$$

683 where δ_A , δ_B , and δ_{A+B} are the relative uncertainties of Part A, Part B, and the total
 684 deposition flux, respectively; U_A , U_B , and U_{A+B} are the absolute uncertainties of them,
 685 respectively; F_{A+B} is the total deposition flux; and P_A and P_B are the proportions of
 686 Part A and Part B deposition fluxes, respectively.

687 Table 1 summarizes the previously estimated relative uncertainties for wet, dry, and
 688 forest Hg deposition fluxes. Although the uncertainty of precipitation Hg deposition
 689 flux is low, the uncertainty of non-precipitation Hg deposition has been neglected.
 690 Due to the condensation effect, non-precipitation deposition could contribute
 691 equivalent or even larger proportion to Hg wet deposition than rainfall (Stankwitz et
 692 al., 2012; Blackwell and Driscoll, 2015b; Weiss-Penzias et al., 2016b; Gerson et al.,
 693 2017). Considering the global area of hotspot regions for cloud, fog, dew, and frost,
 694 such as alpine and coastal regions, the overall contribution of non-precipitation
 695 deposition to Hg wet deposition is approximately 5–10 %. Given the high uncertainty
 696 level of non-precipitation Hg deposition, the overall uncertainties in the observation
 697 and simulation of global Hg wet deposition are estimated to be $\pm(20-35)$ % and $\pm(30-$
 698 $55)$ %, respectively.

699 Hg dry deposition has a much larger uncertainty level than wet deposition from
 700 both observation and simulation perspectives. High GOM deposition fluxes were
 701 exhibited in North America, while high PBM deposition fluxes were found in East
 702 Asia (Wright et al., 2016). Based on the global observation and simulation data
 703 (Wright et al., 2016; Zhang et al., 2016b), the ratio of global GOM dry deposition
 704 over PBM dry deposition could be in the range of 1:1 to 3:1, and the ratio of global
 705 GEM dry deposition over RM (GOM+PBM) dry deposition could be in the range of

706 1:9 to 9:1. Therefore, the overall uncertainties in the observation and simulation of
707 global Hg dry deposition are estimated to be $\pm(50-90)$ % and $\pm(90-130)$ %,
708 respectively.

709 Without studies specifically on throughfall deposition modeling, the uncertainty of
710 throughfall Hg deposition simulation has been estimated based on the uncertainties of
711 both wet and dry deposition simulation, and turned out to be about $\pm(50-90)$ %.
712 Studies on both litterfall and throughfall Hg deposition (Larssen et al., 2008; Navrátil
713 et al., 2014; Luo et al., 2016; Ma et al., 2015; Fu et al., 2016a; Wang et al., 2016a;
714 Gerson et al., 2017) showed that the relative contributions of litterfall and throughfall
715 could be in the range of 2:3 to 4:1. Accordingly, the overall uncertainties in the
716 observation and simulation of global forest Hg deposition are estimated to be $\pm(15-$
717 $25)$ % and $\pm(40-70)$ %, respectively.

718 Based on global and regional modeling studies (Selin and Jacob, 2008; Wang et al.,
719 2016a; UN Environment, 2019), the relative contributions of wet, dry, and litterfall
720 Hg deposition are estimated to be approximately 1:2:1. With the previously estimated
721 uncertainty ranges for wet, dry, and litterfall deposition, the overall uncertainties in
722 the observation and simulation of global total Hg deposition are calculated to be
723 $\pm(25-50)$ % and $\pm(45-70)$ %, respectively. It should be noted that the low overall
724 uncertainty for observation can only be achieved when Hg deposition networks are
725 established worldwide.

726 **6 Implications and future research needs**

727 With a big effort of literature review, this study has estimated the uncertainties in the
728 observation and simulation of global Hg deposition to the land surfaces through
729 different pathways. The implications from the comprehensive uncertainty analysis and
730 the derivative research needs in the future are as follows:

731 (1) The observation methods for both wet and forest Hg deposition fluxes have low
732 uncertainty levels. Although large uncertainties still exist in the methods for Hg dry
733 deposition measurements, the overall uncertainty in global Hg deposition observation
734 can be as low as $\pm(25-50)$ %. Optimized surrogate surfaces and DFCs are economic
735 approaches for RM and GEM measurements, respectively, and could be useful
736 methods for the global dry deposition network.

737 (2) Methods with high time resolution for the accurate measurements of GOM and
738 PBM concentrations are in urgent needs. On account of the GOM dry deposition

739 velocity, the chemical form of GOM also plays a crucial role. Different model
740 parameterizations should be applied for different GOM species. Therefore,
741 quantification methods for measuring different GOM species need to be developed to
742 improve the simulation of GOM dry deposition flux.

743 (3) More comparisons between observation and simulation of the GEM dry
744 deposition flux should be conducted to improve model parameterization. Moreover,
745 the GEM deposition process is complicated in forests. It is useful to measure the
746 above-canopy apparent deposition flux, the under-canopy dry deposition flux, the
747 litterfall deposition flux, and the throughfall deposition flux at the same site to get a
748 more comprehensive understanding of the process.

749 (4) Non-precipitation Hg wet deposition has been neglected in the global
750 monitoring networks and modeling studies. Cloud, fog, or even dew and frost Hg
751 deposition could be quite important in hotspot regions, such as alpine and coastal
752 areas. It could be enriched in aqueous Hg and affect other deposition processes, or in
753 other words, change the overall Hg residence time. Extremely large uncertainties still
754 exist in both observation and simulation of non-precipitation Hg wet deposition. More
755 standardized sampling methods are required for long-term observation of non-
756 precipitation Hg wet deposition.

757 (5) Asia has the highest atmospheric Hg concentration level. However, the Hg
758 deposition studies in Asia are still quite limited. The Hg wet deposition network in
759 Asia is not as mature as in North America and Europe, and there are only a few
760 scattered studies on dry deposition in East Asia. The Hg wet and dry deposition
761 processes in Asia could be quite different from those in North America and Europe
762 because of the high atmospheric Hg and high PM condition in Asia.

763

764 *Data availability.* Data presented in this study were all generated from published
765 literature and are available from the original researchers. Data in this research are
766 available in the supplement.

767

768 *Supplement.* The supplement related to this article is available online at:

769

770 *Author contribution.* Dr. Lei Zhang designed the review framework. Dr. Lei Zhang
771 and Peisheng Zhou did the most literature review work with contributions from

772 Shuzhen Cao and Dr. Yu Zhao. Dr. Lei Zhang prepared the manuscript with
773 contributions from all co-authors.

774

775 *Competing interests.* The authors declare that they have no conflict of interest.

776

777 *Acknowledgements.* This review work was supported by the National Natural Science
778 Foundation of China (No. 21876077) and the Fundamental Research Funds for the
779 Central Universities in China (No. 14380080, No. 14380092, and No. 14380124).

780

781 **References**

782 Aas, W. (Ed.): Data quality 2004, quality assurance, and field comparisons, C587
783 EMEP/CCC-Report 4/2006, NILU, Kjeller, Norway, 2006.

784 Agnan, Y., Le Dantec, T., Moore, C. W., Edwards, G. C., and Obrist, D.: New
785 constraints on terrestrial surface atmosphere fluxes of gaseous elemental mercury
786 using a global database, *Environ. Sci. Technol.*, 50, 507–524,
787 10.1021/acs.est5b04013, 2016.

788 Ahn, M. C., Yi, S. M., Holsen, T. M., and Han, Y. J.: Mercury wet deposition in rural
789 Korea: concentrations and fluxes, *J. Environ. Monit.*, 13, 2748–2754,
790 10.1039/c1em10014a, 2011.

791 Åkerblom, S., Meili, M., and Bishop, K.: Organic matter in rain: an overlooked
792 influence on mercury deposition, *Environ. Sci. Technol. Lett.*, 2, 128–132,
793 10.1021/acs.estlett.5b00009, 2015.

794 Bash, J. O.: Description and initial simulation of a dynamic bidirectional air-surface
795 exchange model for mercury in Community Multiscale Air Quality (CMAQ)
796 model, *J. Geophys. Res.*, 115, 10.1029/2009jd012834, 2010.

797 Baya, A. P., and Van Heyst, B.: Assessing the trends and effects of environmental
798 parameters on the behaviour of mercury in the lower atmosphere over cropped
799 land over four seasons, *Atmos. Chem. Phys.*, 10, 8617–8628, 10.5194/acp-10-
800 8617-2010, 2010.

801 Benoit, J. M., Cato, D. A., Denison, K. C., and Moreira, A. E.: Seasonal mercury
802 dynamics in a New England vernal pool, *Wetlands*, 33, 887–894,
803 10.1007/s13157-013-0447-4, 2013.

804 Bieser, J., De Simone, F., Gencarelli, C., Geyer, B., Hedgecock, I., Matthias, V.,

805 Travnikov, O., and Weigelt, A.: A diagnostic evaluation of modeled mercury wet
806 depositions in Europe using atmospheric speciated high-resolution observations,
807 *Environ. Sci. Pollut. Res.*, 21, 9995–10012, 10.1007/s11356-014-2863-2, 2014.

808 Blackwell, B. D., and Driscoll, C. T.: Using foliar and forest floor mercury
809 concentrations to assess spatial patterns of mercury deposition, *Environ. Pollut.*,
810 202, 126–134, 10.1016/j.envpol.2015.02.036, 2015a.

811 Blackwell, B. D., and Driscoll, C. T.: Deposition of mercury in forests along a
812 montane elevation gradient, *Environ. Sci. Technol.*, 49, 5363–5370,
813 10.1021/es505928w, 2015b.

814 Brunke, E.-G., Walters, C., Mkololo, T., Martin, L., Labuschagne, C., Silwana, B.,
815 Slemr, F., Weigelt, A., Ebinghaus, R., and Somerset, V.: Mercury in the
816 atmosphere and in rainwater at Cape Point, South Africa, *Atmos. Environ.*, 125,
817 24–32, 10.1016/j.atmosenv.2015.10.059, 2016.

818 Buch, A. C., Correia, M. E., Teixeira, D. C., and Silva-Filho, E. V.: Characterization
819 of soil fauna under the influence of mercury atmospheric deposition in Atlantic
820 Forest, Rio de Janeiro, Brazil, *J. Environ. Sci.*, 32, 217–227,
821 10.1016/j.jes.2015.01.009, 2015.

822 Bullock, O. R., Atkinson, D., Braverman, T., Civerolo, K., Dastoor, A., Davignon, D.,
823 Ku, J. Y., Lohman, K., Myers, T. C., Park, R. J., Seigneur, C., Selin, N. E., Sistla,
824 G., and Vijayaraghavan, K.: The North American Mercury Model
825 Intercomparison Study (NAMMIS): Study description and model-to-model
826 comparisons, *J. Geophys. Res.-Atmos.*, 113, D17310,
827 doi:10.1029/2008jd009803, 2008

828 Bullock, O. R., Atkinson, D., Braverman, T., Civerolo, K., Dastoor, A., Davignon, D.,
829 Ku, J.-Y., Lohman, K., Myers, T. C., Park, R. J., Seigneur, C., Selin, N. E., Sistla,
830 G., and Vijayaraghavan, K.: An analysis of simulated wet deposition of mercury
831 from the North American Mercury Model Intercomparison Study, *J. Geophys.*
832 *Res.-Atmos.*, 114, D08301, doi:10.1029/2008jd011224, 2009.

833 Bushey, J. T., Nallana, A. G., Montesdeoca, M. R., and Driscoll, C. T.: Mercury
834 dynamics of a northern hardwood canopy, *Atmos. Environ.*, 42, 6905–6914,
835 10.1016/j.atmosenv.2008.05.043, 2008.

836 Castelle, S., Schäfer, J., Blanc, G., Dabrin, A., Lanceleur, L., and Masson, M.:
837 Gaseous mercury at the air–water interface of a highly turbid estuary (Gironde
838 Estuary, France), *Mar. Chem.*, 117, 42–51, 10.1016/j.marchem.2009.01.005,

839 2009.

840 Castro, M. S., Moore, C., Sherwell, J., and Brooks, S. B.: Dry deposition of gaseous
841 oxidized mercury in Western Maryland, *Sci. Total Environ.*, 417–418, 232–240,
842 10.1016/j.scitotenv.2011.12.044, 2012.

843 Chen, L., Li, Y., Liu, C., Guo, L., and Wang, X.: Wet deposition of mercury in
844 Qingdao, a coastal urban city in China: Concentrations, fluxes, and influencing
845 factors, *Atmos. Environ.*, 174, 204–213, 10.1016/j.atmosenv.2017.11.059, 2018.

846 Cheng, I., Zhang, L., and Mao, H.: Relative contributions of gaseous oxidized
847 mercury and fine and coarse particle-bound mercury to mercury wet deposition
848 at nine monitoring sites in North America, *J. Geophys. Res. Atmos.*, 120, 8549–
849 8562, 10.1002/2015jd023769, 2015.

850 Cheng, I. and Zhang, L.: Uncertainty assessment of gaseous oxidized mercury
851 measurements collected by Atmospheric Mercury Network, *Environ. Sci.*
852 *Technol.*, 51, 855–862, 2017.

853 Cheng, Z. L., Luo, Y., Zhang, T., and Duan, L.: Deposition of Sulfur, Nitrogen and
854 Mercury in Two Typical Forest Ecosystems in Southern China, *Environ. Sci.*,
855 2017.

856 Choi, H.-D., Sharac, T. J., and Holsen, T. M.: Mercury deposition in the Adirondacks:
857 A comparison between precipitation and throughfall, *Atmos. Environ.*, 42, 1818–
858 1827, 10.1016/j.atmosenv.2007.11.036, 2008.

859 Ci, Z., Peng, F., Xue, X., and Zhang, X.: Air–surface exchange of gaseous mercury
860 over permafrost soil: an investigation at a high-altitude (4700 m a.s.l.) and
861 remote site in the central Qinghai–Tibet Plateau, *Atmos. Chem. Phys.*, 16,
862 14741–14754, 10.5194/acp-16-14741-2016, 2016.

863 Ci, Z. J., Zhang, X. S., and Wang, Z. W.: Enhancing atmospheric mercury research in
864 China to improve the current understanding of the global mercury cycle: The
865 need for urgent and closely coordinated efforts, *Environ. Sci. Technol.*, 46, 5636–
866 5642, 2012.

867 Connan, O., Maro, D., Hébert, D., Roupsard, P., Goujon, R., Letellier, B., and Le
868 Cavelier, S.: Wet and dry deposition of particles associated metals (Cd, Pb, Zn,
869 Ni, Hg) in a rural wetland site, Marais Vernier, France, *Atmos. Environ.*, 67,
870 394–403, 10.1016/j.atmosenv.2012.11.029, 2013.

871 Converse, A. D., Riscassi, A. L., and Scanlon, T. M.: Seasonal variability in gaseous
872 mercury fluxes measured in a high-elevation meadow, *Atmos. Environ.*, 44,

873 2176–2185, 10.1016/j.atmosenv.2010.03.024, 2010.

874 Converse, A. D., Riscassi, A. L., and Scanlon, T. M.: Seasonal contribution of dewfall
875 to mercury deposition determined using a micrometeorological technique and
876 dew chemistry, *J. Geophys. Res. Atmos.*, 119(1), 284–292,
877 doi:10.1002/2013JD020491, 2014.

878 Dastoor, A. P., and Larocque, Y.: Global circulation of atmospheric mercury: a
879 modelling study, *Atmos. Environ.*, 38, 147–161,
880 10.1016/j.atmosenv.2003.08.037, 2004.

881 Dutt, U., Nelson, P. F., Morrison, A. L., and Strezov, V.: Mercury wet deposition and
882 coal-fired power station contributions: An Australian study, *Fuel Process.*
883 *Technol.*, 90, 1354–1359, 10.1016/j.fuproc.2009.06.019, 2009.

884 Enrico, M., Roux, G. L., Maruszczak, N., Heimbürger, L. E., Claustres, A., Fu, X., Sun,
885 R., and Sonke, J. E.: Atmospheric mercury transfer to peat bogs dominated by
886 gaseous elemental mercury dry deposition, *Environ. Sci. Technol.*, 50, 2405–
887 2412, 10.1021/acs.est.5b06058, 2016.

888 EPA Method 1631: [http://water.epa.gov/scitech/methods/cwa/
889 metals/mercury/index.cfm](http://water.epa.gov/scitech/methods/cwa/metals/mercury/index.cfm), last access: 27 December 2014.

890 Fang, G.-C., Tsai, J.-H., Lin, Y.-H., and Chang, C.-Y.: Dry deposition of atmospheric
891 particle-bound mercury in the Middle Taiwan, *Aerosol Air Qual. Res.*, 12, 1298–
892 1308, 10.4209/aaqr.2012.04.0093, 2012a.

893 Fang, G.-C., Lin, Y.-H., and Chang, C.-Y.: Use of mercury dry deposition samplers to
894 quantify dry deposition of particulate-bound mercury and reactive gaseous
895 mercury at a traffic sampling site, *Environ. Forensics*, 14, 182–186,
896 10.1080/15275922.2013.814177, 2013.

897 Fang, G. C., Zhang, L., and Huang, C. S.: Measurements of size-fractionated
898 concentration and bulk dry deposition of atmospheric particulate bound mercury,
899 *Atmos. Environ.*, 61, 371–377, 10.1016/j.atmosenv.2012.07.052, 2012b.

900 Fernandez, D., Torregrosa, A., Weiss-Penzias, P., Zhang, B.J., Sorensen, D., Cohen,
901 R.E., McKinley, G.H., Kleingartner, L., Oliphant, A., Bowman, M.: Fog Water
902 Collection Effectiveness: Mesh Intercomparisons, *Aerosol Air Qual. Res.*, 18,
903 270–283, 10.4209/aaqr.2017.01.0040, 2018.

904 Fisher, L. S., and Wolfe, M. H.: Examination of mercury inputs by throughfall and
905 litterfall in the Great Smoky Mountains National Park, *Atmos. Environ.*, 47,
906 554–559, 10.1016/j.atmosenv.2011.10.017, 2012.

907 Fostier, A. H., Melendez-Perez, J. J., and Richter, L.: Litter mercury deposition in the
908 Amazonian rainforest, *Environ. Pollut.*, 206, 605–610,
909 10.1016/j.envpol.2015.08.010, 2015.

910 Fragoso, C. P., Bernini, E., Araújo, B. F., Almeida, M. G. d., and Rezende, C. E. d.:
911 Mercury in litterfall and sediment using elemental and isotopic composition of
912 carbon and nitrogen in the mangrove of Southeastern Brazil, *Estuarine Coastal
913 And Shelf Science*, 202, 30–39, 10.1016/j.ecss.2017.12.005, 2018.

914 Fritsche, J., Obrist, D., Zeeman, M., Conen, F., Eugster, W., and Alewell, C.:
915 Elemental mercury fluxes over a sub-alpine grassland determined with two
916 micrometeorological methods, *Atmos. Environ.*, 42, 2922–2933,
917 10.1016/j.atmosenv.2007.12.055, 2008.

918 Fu, X., Feng, X., Zhu, W., Zheng, W., Wang, S., and Lu, J. Y.: Total particulate and
919 reactive gaseous mercury in ambient air on the eastern slope of the Mt. Gongga
920 area, China, *Appl. Geochem.*, 23, 408–418, 10.1016/j.apgeochem.2007.12.018,
921 2008.

922 Fu, X., Feng, X., Zhu, W., Rothenberg, S., Yao, H., and Zhang, H.: Elevated
923 atmospheric deposition and dynamics of mercury in a remote upland forest of
924 southwestern China, *Environ. Pollut.*, 158, 2324–2333,
925 10.1016/j.envpol.2010.01.032, 2010a.

926 Fu, X. W., Feng, X., Dong, Z. Q., Yin, R. S., Wang, J. X., Yang, Z. R., and Zhang, H.:
927 Atmospheric gaseous elemental mercury (GEM) concentrations and mercury
928 depositions at a high-altitude mountain peak in south China, *Atmos. Chem.
929 Phys.*, 10, 2425–2437, DOI 10.5194/acp-10-2425-2010, 2010b.

930 Fu, X., Feng, X., Sommar, J., and Wang, S.: A review of studies on atmospheric
931 mercury in China, *Sci. Total Environ.*, 421–422, 73–81,
932 10.1016/j.scitotenv.2011.09.089, 2012.

933 Fu, X., Yang, X., Lang, X., Zhou, J., Zhang, H., Yu, B., Yan, H., Lin, C.-J., and Feng,
934 X.: Atmospheric wet and litterfall mercury deposition at urban and rural sites in
935 China, *Atmos. Chem. Phys.*, 16, 11547–11562, 10.5194/acp-16-11547-2016,
936 2016a.

937 Fu, X., Maruschak, N., Heimbürger, L.-E., Sauvage, B., Gheusi, F., Prestbo, E. M.,
938 and Sonke, J. E.: Atmospheric mercury speciation dynamics at the high-altitude
939 Pic du Midi Observatory, southern France, *Atmos. Chem. Phys.*, 16, 5623–5639,
940 <https://doi.org/10.5194/acp-16-5623-2016>, 2016b.

941 Gerson, J. R., Driscoll, C. T., Demers, J. D., Sauer, A. K., Blackwell, B. D.,
942 Montesdeoca, M. R., Shanley, J. B., and Ross, D. S.: Deposition of mercury in
943 forests across a montane elevation gradient: Elevational and seasonal patterns in
944 methylmercury inputs and production, *J. Geophys. Res. Biogeo.*, 122, 1922–
945 1939, 10.1002/2016jg003721, 2017.

946 Gichuki, S. W., and Mason, R. P.: Mercury and metals in South African precipitation,
947 *Atmos. Environ.*, 79, 286–298, 10.1016/j.atmosenv.2013.04.009, 2013.

948 Gichuki, S. W., and Mason, R. P.: Wet and dry deposition of mercury in Bermuda,
949 *Atmos. Environ.*, 87, 249–257, 10.1016/j.atmosenv.2014.01.025, 2014.

950 Gong, P., Wang, X. P., Xue, Y. G., Xu, B. Q., and Yao, T. D.: Mercury distribution in
951 the foliage and soil profiles of the Tibetan forest: processes and implications for
952 regional cycling, *Environ. Pollut.*, 188, 94–101, 10.1016/j.envpol.2014.01.020,
953 2014.

954 Gratz, L. E., and Keeler, G. J.: Sources of mercury in precipitation to Underhill, VT,
955 *Atmos. Environ.*, 45, 5440–5449, 10.1016/j.atmosenv.2011.07.001, 2011.

956 Guo, J., Kang, S., Huang, J., Zhang, Q., Rupakheti, M., Sun, S., Tripathi, L.,
957 Rupakheti, D., Panday, A. K., Sillanpaa, M., and Paudyal, R.: Characterizations
958 of atmospheric particulate-bound mercury in the Kathmandu Valley of Nepal,
959 South Asia, *Sci. Total Environ.*, 579, 1240–1248,
960 10.1016/j.scitotenv.2016.11.110, 2017.

961 Guo, Y., Feng, X., Li, Z., He, T., Yan, H., Meng, B., Zhang, J., and Qiu, G.:
962 Distribution and wet deposition fluxes of total and methyl mercury in Wujiang
963 River Basin, Guizhou, China, *Atmos. Environ.*, 42, 7096–7103,
964 10.1016/j.atmosenv.2008.06.006, 2008.

965 Gustin, M. S., Lindberg, S. E., and Weisberg, P. J.: An update on the natural sources
966 and sinks of atmospheric mercury, *Appl. Geochem.*, 23, 482–493,
967 10.1016/j.apgeochem.2007.12.010, 2008.

968 Gustin, M. S., Weiss-Penzias, P. S., and Peterson, C.: Investigating sources of gaseous
969 oxidized mercury in dry deposition at three sites across Florida, USA, *Atmos.*
970 *Chem. Phys.*, 12, 9201–9219, 10.5194/acp-12-9201-2012, 2012.

971 Gustin, M. S., Huang, J., Miller, M. B., Peterson, C., Jaffe, D. A., Ambrose, J., Finley,
972 B. D., Lyman, S. N., Call, K., Talbot, R., Feddersen, D., Mao, H., and Lindberg,
973 S. E.: Do we understand what the mercury speciation instruments are actually
974 measuring? Results of RAMIX, *Environ. Sci. Technol.*, 47, 7295–7306,

975 10.1021/es3039104, 2013.

976 Gustin, M. S., Amos, H. M., Huang, J., Miller, M. B., and Heidecorn, K.: Measuring
977 and modeling mercury in the atmosphere: a critical review, *Atmos. Chem. Phys.*,
978 15, 5697–5713, 10.5194/acp-15-5697-2015, 2015.

979 Hall, N. L., Dvornch, J. T., Marsik, F. J., Barres, J. A., and Landis, M. S.: An artificial
980 turf-based surrogate surface collector for the direct measurement of atmospheric
981 mercury dry deposition, *Int. J. Environ. Res. Public Health*, 14,
982 10.3390/ijerph14020173, 2017.

983 Han, J.-S., Seo, Y.-S., Kim, M.-K., Holsen, T. M., and Yi, S.-M.: Total atmospheric
984 mercury deposition in forested areas in South Korea, *Atmos. Chem. Phys.*, 16,
985 7653–7662, 10.5194/acp-16-7653-2016, 2016.

986 Hansen, A. M., and Gay, D. A.: Observations of mercury wet deposition in Mexico,
987 *Environ. Sci. Pollut. Res. Int.*, 20, 8316–8325, 10.1007/s11356-013-2012-3,
988 2013.

989 Holloway, T., Voigt, C., Morton, J., Spak, S. N., Rutter, A. P., and Schauer, J. J.: An
990 assessment of atmospheric mercury in the Community Multiscale Air Quality
991 (CMAQ) model at an urban site and a rural site in the Great Lakes Region of
992 North America, *Atmos. Chem. Phys.*, 12, 7117–7133, doi:10.5194/acp-12-7117-
993 2012, 2012.

994 Holmes, H. A., Pardyjak, E. R., Perry, K. D., and Abbott, M. L.: Gaseous dry
995 deposition of atmospheric mercury: A comparison of two surface resistance
996 models for deposition to semiarid vegetation, *J. Geophys. Res.*, 116,
997 10.1029/2010jd015182, 2011.

998 Horowitz, H. M., Jacob, D. J., Zhang, Y., Dibble, T. S., Slemr, F., Amos, H. M.,
999 Schmidt, J. A., Corbitt, E. S., Marais, E. A., and Sunderland, E. M.: A new
1000 mechanism for atmospheric mercury redox chemistry: implications for the global
1001 mercury budget, *Atmos. Chem. Phys.*, 17, 6353–6371,
1002 <https://doi.org/10.5194/acp-17-6353-2017>, 2017.

1003 Huang, J., Choi, H. D., Landis, M. S., and Holsen, T. M.: An application of passive
1004 samplers to understand atmospheric mercury concentration and dry deposition
1005 spatial distributions, *J Environ Monit*, 14, 2976-2982, 10.1039/c2em30514c,
1006 2012a.

1007 Huang, J., Kang, S. C., Zhang, Q. G., Yan, H. Y., Guo, J. M., Jenkins, M. G., Zhang,
1008 G. S., and Wang, K.: Wet deposition of mercury at a remote site in the Tibetan

1009 Plateau: Concentrations, speciation, and fluxes, *Atmos. Environ.*, 62, 540–550,
1010 10.1016/j.atmosenv.2012.09.003, 2012b.

1011 Huang, J., Kang, S., Wang, S., Wang, L., Zhang, Q., Guo, J., Wang, K., Zhang, G.,
1012 and Tripathee, L.: Wet deposition of mercury at Lhasa, the capital city of Tibet,
1013 *Sci. Total Environ.*, 447, 123–132, 10.1016/j.scitotenv.2013.01.003, 2013a.

1014 Huang, J. Y., Miller, M. B., Weiss-Penzias, P., and Gustin, M. S.: Comparison of
1015 Gaseous Oxidized Hg Measured by KCl-Coated Denuders, and Nylon and
1016 Cation Exchange Membranes, *Environ. Sci. Technol.*, 47, 7307–7316, 2013b.

1017 Huang, J., and Gustin, M. S.: Use of passive sampling methods and models to
1018 understand sources of mercury deposition to high elevation sites in the Western
1019 United States, *Environ. Sci. Technol.*, 49, 432–441, 10.1021/es502836w, 2015a.

1020 Huang, J., Lyman, S. N., Hartman, J. S., and Gustin, M. S.: A review of passive
1021 sampling systems for ambient air mercury measurements, *Environ. Sci.:*
1022 *Processes Impacts*, 16, 374–392, 10.1039/c3em00501a, 2014.

1023 Huang, J., and Gustin, M. S.: Uncertainties of gaseous oxidized mercury
1024 measurements using KCl-coated denuders, cation-exchange membranes, and
1025 nylon membranes: Humidity influences, *Environ. Technol.*, 49, 6102–6108,
1026 10.1021/acs.est.5b00098, 2015b.

1027 Huang, J., Kang, S., Zhang, Q., Guo, J., Sillanpaa, M., Wang, Y., Sun, S., Sun, X., and
1028 Tripathee, L.: Characterizations of wet mercury deposition on a remote high-
1029 elevation site in the southeastern Tibetan Plateau, *Environ. Pollut.*, 206, 518–526,
1030 10.1016/j.envpol.2015.07.024, 2015.

1031 Huang, J., Kang, S., Guo, J., Zhang, Q., Cong, Z., Sillanpää, M., Zhang, G., Sun, S.,
1032 and Tripathee, L.: Atmospheric particulate mercury in Lhasa city, Tibetan
1033 Plateau, *Atmos. Environ.*, 142, 433–441, 10.1016/j.atmosenv.2016.08.021, 2016.

1034 Huang, J. Y., Miller, M. B., Edgerton, E., and Gustin, M. S.: Deciphering potential
1035 chemical compounds of gaseous oxidized mercury in Florida, USA, *Atmos.*
1036 *Chem. Phys.*, 17, 1689–1698, 10.5194/acp-17-1689-2017, 2017.

1037 Jaffe, D. A., Lyman, S., Amos, H. M., Gustin, M. S., Huang, J., Selin, N. E., Levin, L.,
1038 ter Schure, A., Mason, R. P., Talbot, R., Rutter, A., Finley, B., Jaeglé, L., Shah,
1039 V., McClure, C., Ambrose, J., Gratz, L., Lindberg, S., Weiss-Penzias, P., Sheu,
1040 G.-R., Feddersen, D., Horvat, M., Dastoor, A., Hynes, A. J., Mao, H., Sonke, J.
1041 E., Slemr, F., Fisher, J. A., Ebinghaus, R., Zhang, Y., and Edwards, G.: Progress
1042 on Understanding Atmospheric Mercury Hampered by Uncertain Measurements,

1043 Environ. Sci. Technol., 48, 7204–7206, doi:10.1021/es5026432, 2014.

1044 Juillerat, J. I., Ross, D. S., and Bank, M. S.: Mercury in litterfall and upper soil
1045 horizons in forested ecosystems in Vermont, USA, Environ. Toxicol. Chem., 31,
1046 1720–1729, 10.1002/etc.1896, 2012.

1047 Katata, G.: Fogwater deposition modeling for terrestrial ecosystems: A review of
1048 developments and measurements, J Geophys Res-Atmos, 119, Artn
1049 2014jd02166910.1002/2014jd021669, 2014.

1050 Kim, M.-G., Lee, B.-K., and Kim, H.-J.: Cloud/fog water chemistry at a high
1051 elevation site in South Korea, J. Atmos. Chem., 55, 13–29, 10.1007/s10874-005-
1052 9004-8, 2006.

1053 Lai, S. O., Huang, J., Hopke, P. K., and Holsen, T. M.: An evaluation of direct
1054 measurement techniques for mercury dry deposition, Sci. Total Environ., 409,
1055 1320–1327, 10.1016/j.scitotenv.2010.12.032, 2011.

1056 Larssen, T., de Wit, H. A., Wiker, M., and Halse, K.: Mercury budget of a small
1057 forested boreal catchment in southeast Norway, Sci. Total Environ., 404, 290–
1058 296, 10.1016/j.scitotenv.2008.03.013, 2008.

1059 Lawson, S. T., Scherbatskoy, T. D., Malcolm, E. G., and Keeler, G. J.: Cloud water
1060 and throughfall deposition of mercury and trace elements in a high elevation
1061 spruce–fir forest at Mt. Mansfield, Vermont, J. Environ. Monit., 5, 578–583,
1062 10.1039/b210125d, 2003.

1063 Lin, C.-J., Pongprueksa, P., Lindberg, S. E., Pehkonen, S. O., Byun, D., and Jang, C.:
1064 Scientific uncertainties in atmospheric mercury models I: Model science
1065 evaluation, Atmos. Environ., 40, 2911–2928, 2006.

1066 Lin, C.-J., Pongprueksa, P., Lindberg, S. E., Pehkonen, S. O., Jang, C., Braverman, T.,
1067 and Ho, T. C.: Scientific uncertainties in atmospheric mercury models II:
1068 Sensitivity analysis in the CONUS domain, Atmos. Environ., 41, 6544–6560,
1069 2007.

1070 Lin, C.-J., Pan, L., Streets, D. G., Shetty, S. K., Jang, C., Feng, X., Chu, H.-W., and
1071 Ho, T. C.: Estimating mercury emission outflow from East Asia using CMAQ-
1072 Hg, Atmos. Chem. Phys., 10, 1853–1864, doi:10.5194/acp-10-1853-2010, 2010.

1073 Lindberg, S. E., Bullock, R., Ebinghaus, R., Engstrom, D., Feng, X. B., Fitzgerald,
1074 W., Pirrone, N., Prestbo, E., and Seigneur, C.: A synthesis of progress and
1075 uncertainties in attributing the sources of mercury in deposition, Ambio, 36, 19–
1076 32, 2007.

1077 Lindberg, S. and Meyers, T.: Development of an automated micrometeorological
1078 method for measuring the emission of mercury vapor from wetland vegetation,
1079 *Wetl. Ecol. Manag.*, 9, 333–347, 2001.

1080 Lombard, M. A. S., Bryce, J. G., Mao, H., and Talbot, R.: Mercury deposition in
1081 Southern New Hampshire, 2006–2009, *Atmos. Chem. Phys.*, 11, 7657–7668,
1082 10.5194/acp-11-7657-2011, 2011.

1083 Lu, A., and Liu, H.: Study on the time distribution characteristics and source of wet
1084 deposition mercury in weinan city, *Journal of Arid Land Resources and*
1085 *Environment*, 2018.

1086 Luo, Y., Duan, L., Driscoll, C. T., Xu, G. Y., Shao, M. S., Taylor, M., Wang, S. X., and
1087 Hao, J. M.: Foliage/atmosphere exchange of mercury in a subtropical coniferous
1088 forest in south China, *J. Geophys. Res. Biogeo.*, 121, 2006–2016,
1089 10.1002/2016jg003388, 2016.

1090 Lyman, S. N., Gustin, M. S., Prestbo, E. M., and Marsik, F. J.: Estimation of dry
1091 deposition of atmospheric mercury in Nevada by direct and indirect methods,
1092 *Environ. Sci. Technol.*, 41, 1970–1976, 2007.

1093 Lyman, S. N., Gustin, M. S., Prestbo, E. M., Kilner, P. I., Edgerton, E., and Hartsell,
1094 B.: Testing and application of surrogate surfaces for understanding potential
1095 gaseous oxidized mercury dry deposition, *Environ. Sci. Technol.*, 43, 6235–6241,
1096 2009.

1097 Lyman, S. N., Jaffe, D. A., and Gustin, M. S.: Release of mercury halides from KCl
1098 denuders in the presence of ozone, *Atmos. Chem. Phys.*, 10, 8197–8204,
1099 10.5194/acp-10-8197-2010, 2010.

1100 Lynam, M., Dvonch, J. T., Barres, J., and Percy, K.: Atmospheric wet deposition of
1101 mercury to the Athabasca Oil Sands Region, Alberta, Canada, *Air Qual. Atmos.*
1102 *Health*, 11, 83–93, 10.1007/s11869-017-0524-6, 2017.

1103 Lynam, M. M., Dvonch, J. T., Hall, N. L., Morishita, M., and Barres, J. A.: Spatial
1104 patterns in wet and dry deposition of atmospheric mercury and trace elements in
1105 central Illinois, USA, *Environ. Sci. Pollut. Res. Int.*, 21, 4032–4043,
1106 10.1007/s11356-013-2011-4, 2014.

1107 Ma, M., Wang, D., Du, H., Sun, T., Zhao, Z., and Wei, S.: Atmospheric mercury
1108 deposition and its contribution of the regional atmospheric transport to mercury
1109 pollution at a national forest nature reserve, southwest China, *Environ. Sci.*
1110 *Pollut. Res. Int.*, 22, 20007–20018, 10.1007/s11356-015-5152-9, 2015.

1111 Ma, M., Wang, D., Du, H., Sun, T., Zhao, Z., Wang, Y., and Wei, S.: Mercury
1112 dynamics and mass balance in a subtropical forest, southwestern China, *Atmos.*
1113 *Chem. Phys.*, 16, 4529–4537, 10.5194/acp-16-4529-2016, 2016.

1114 Malcolm, E. G. and Keeler, G. J.: Measurements of Mercury in Dew: Atmospheric
1115 Removal of Mercury Species to a Wetted Surface, *Environ. Sci. Technol.*, 36,
1116 2815–2821, <https://doi.org/10.1021/es011174z>, 2002.

1117 Malcolm, E. G., Keeler, G. J., Lawson, S. T., and Sherbatskoy, T. D.: Mercury and
1118 trace elements in cloud water and precipitation collected on Mt. Mansfield,
1119 Vermont, *J. Environ. Monit.*, 5, 584, 10.1039/b210124f, 2003.

1120 Marsik, F. J., Keeler, G. J., and Landis, M. S.: The dry-deposition of speciated
1121 mercury to the Florida Everglades: Measurements and modeling, *Atmos.*
1122 *Environ.*, 41, 136–149, 10.1016/j.atmosenv.2006.07.032, 2007.

1123 Marumoto, K., and Matsuyama, A.: Mercury speciation in wet deposition samples
1124 collected from a coastal area of Minamata Bay, *Atmos. Environ.*, 86, 220–227,
1125 10.1016/j.atmosenv.2013.12.011, 2014.

1126 McClure, C. D., Jaffe, D. A., and Edgerton, E. S.: Evaluation of the KCl denuder
1127 method for gaseous oxidized mercury using HgBr₂ at an in-service AMNet site,
1128 *Environ. Sci. Technol.*, 48, 11437–11444, 10.1021/es502545k, 2014.

1129 Meier, C.E., Stanturf, J.A., Gardiner, E.S.: Litterfall in the hardwood forest of a minor
1130 alluvial floodplain. *For. Ecol. Manag.* 234, 60-57, 10.1016/j.foreco.2006.06.026,
1131 2006.

1132 Meyers, T. P., Hall, M. E., Lindberg, S. E., and Kim, K.: Use of the modified Bowen-
1133 ratio technique to measure fluxes of trace gases, *Atmos. Environ.*, 30, 3321–
1134 3329, 1996.

1135 Miller, M. B., Gustin, M. S., and Eckley, C. S.: Measurement and scaling of air-
1136 surface mercury exchange from substrates in the vicinity of two Nevada gold
1137 mines, *Sci. Total Environ.*, 409, 3879–3886, 10.1016/j.scitotenv.2011.05.040,
1138 2011.

1139 Montecinos, S., Carvajal, D., and Cereceda, P., Concha, m.: Collection efficiency of
1140 fog events, *Atmos. Res.*, 209, 163–169, 10.1016/j.atmosres.2018.04.004, 2018.

1141 Navrátil, T., Shanley, J., Rohovec, J., Hojdová, M., Penížek, V., and Buchtová, J.:
1142 Distribution and pools of mercury in Czech forest soils, *Water Air and Soil*
1143 *Pollution*, 225, 10.1007/s11270-013-1829-1, 2014.

1144 Nguyen, D. L., Kim, J. Y., Shim, S. G., Ghim, Y. S., and Zhang, X. S.: Shipboard and

1145 ground measurements of atmospheric particulate mercury and total mercury in
1146 precipitation over the Yellow Sea region, *Environ. Pollut.*, 219, 262–274,
1147 10.1016/j.envpol.2016.10.020, 2016.

1148 Obrist, D., Johnson, D. W., and Lindberg, S. E.: Mercury concentrations and pools in
1149 four Sierra Nevada forest sites, and relationships to organic carbon and nitrogen,
1150 *Biogeosciences*, 6, 765–777, DOI 10.5194/bg-6-765-2009, 2009.

1151 Obrist, D., Johnson, D. W., and Edmonds, R. L.: Effects of vegetation type on
1152 mercury concentrations and pools in two adjacent coniferous and deciduous
1153 forests, *Journal of Plant Nutrition and Soil Science*, 175, 68–77,
1154 10.1002/jpln.201000415, 2012.

1155 Obrist, D., Kirk, J. L., Zhang, L., Sunderland, E. M., Jiskra, M., and Selin, N. E.: A
1156 review of global environmental mercury processes in response to human and
1157 natural perturbations: Changes of emissions, climate, and land use, *Ambio*, 47,
1158 116–140, 10.1007/s13280-017-1004-9, 2018.

1159 Peterson, C., Alishahi, M., and Gustin, M. S.: Testing the use of passive sampling
1160 systems for understanding air mercury concentrations and dry deposition across
1161 Florida, USA, *Sci. Total Environ.*, 424, 297–307,
1162 10.1016/j.scitotenv.2012.02.031, 2012.

1163 Poissant, L., Pilote, M., Xu, X., and Zhang, H.: Atmospheric mercury speciation and
1164 deposition in the Bay St. Francois wetlands, *J. Geophys. Res.*, 109, D11301,
1165 doi:10.1029/2003JD004364,2004.

1166 Poissant, L., Pilote, M., Yumvihoze, E., and Lean, D.: Mercury concentrations and
1167 foliage/atmosphere fluxes in a maple forest ecosystem in Quebec, Canada, *J.*
1168 *Geophys. Res.-Atmos.*, 113, 10307–10319,
1169 <https://doi.org/10.1029/2007jd009510>, 2008.

1170 Prestbo, E. M., and Gay, D. A.: Wet deposition of mercury in the US and Canada,
1171 1996–2005: Results and analysis of the NADP mercury deposition network
1172 (MDN), *Atmos. Environ.*, 43, 4223–4233, 10.1016/j.atmosenv.2009.05.028,
1173 2009.

1174 Qin, C., Wang, Y., Peng, Y., and Wang, D.: Four-year record of mercury wet
1175 deposition in one typical industrial city in southwest China, *Atmos. Environ.*,
1176 142, 442–451, 10.1016/j.atmosenv.2016.08.016, 2016.

1177 Richardson, J. B., and Friedland, A. J.: Mercury in coniferous and deciduous upland
1178 forests in Northern New England, USA: implications from climate change,

1179 Biogeosciences, 12, 11463–11498, 10.5194/bgd-12-11463-2015, 2015.

1180 Risch, M. R., DeWild, J. F., Krabbenhoft, D. P., Kolka, R. K., and Zhang, L.: Mercury
1181 in Litterfall at Selected National Atmospheric Deposition Program Mercury
1182 Deposition Network Sites in the Eastern United States, 2007–2009, Environ.
1183 Pollut., 161, 284–290, 2012.

1184 Risch, M., and Kenski, D.: Spatial Patterns and Temporal Changes in Atmospheric-
1185 Mercury Deposition for the Midwestern USA, 2001–2016, Atmosphere, 9, 29,
1186 10.3390/atmos9010029, 2018.

1187 Risch, M. R., DeWild, J. F., Gay, D. A., Zhang, L., Boyer, E. W., and Krabbenhoft, D.
1188 P.: Atmospheric mercury deposition to forests in the eastern USA, Environ.
1189 Pollut., 228, 8–18, 10.1016/j.envpol.2017.05.004, 2017.

1190 Ritchie, C. D., Richards, W., and Arp, P. A.: Mercury in fog on the Bay of Fundy
1191 (Canada), Atmos. Environ., 40, 6321–6328,
1192 <https://doi.org/10.1016/j.atmosenv.2006.05.057>, 2006.

1193 Rutter, A. P., and Schauer, J. J.: The effect of temperature on the gas-particle
1194 partitioning of reactive mercury in atmospheric aerosols, Atmos. Environ., 41,
1195 8647–8657, <https://doi.org/10.1016/j.atmosenv.2007.07.024>, 2007.

1196 Sather, M. E., Mukerjee, S., Smith, L., Mathew, J., Jackson, C., Callison, R., Scrapper,
1197 L., Hathcoat, A., Adam, J., Keese, D., Ketcher, P., Brunette, R., Karlstrom, J.,
1198 and Van der Jagt, G.: Gaseous oxidized mercury dry deposition measurements in
1199 the Four Corners area and Eastern Oklahoma, U.S.A, Atmos. Pollut. Res., 4,
1200 168–180, 10.5094/apr.2013.017, 2013.

1201 Sather, M. E., Mukerjee, S., Allen, K. L., Smith, L., Mathew, J., Jackson, C., Callison,
1202 R., Scrapper, L., Hathcoat, A., Adam, J., Keese, D., Ketcher, P., Brunette, R.,
1203 Karlstrom, J., and Van der Jagt, G.: Gaseous oxidized mercury dry deposition
1204 measurements in the southwestern USA: A comparison between Texas, Eastern
1205 Oklahoma, and the Four Corners Area, Sci. World J., 2014, 580723,
1206 10.1155/2014/580723, 2014.

1207 Schroeder, W. H., and Munthe, J.: Atmospheric mercury - An overview, Atmos.
1208 Environ., 32, 809–822, 1998.

1209 Schwab, J. J., Casson, P., Brandt, R., Husain, L., Dutkewicz, V., Wolfe, D., Demerjian,
1210 K. L., Civerolo, K. L., Rattigan, O. V., Felton, H. D., and Dukett, J. E.:
1211 Atmospheric chemistry measurements at Whiteface Mountain, NY: Cloud water
1212 chemistry, precipitation chemistry, and particulate matter, Aerosol Air Qual. Res.,

1213 16, 841–854, 10.4209/aaqr.2015.05.0344, 2016.

1214 Selin, N. E. and Jacob, D. J.: Seasonal and spatial patterns of mercury wet deposition
1215 in the United States: Constraints on the contribution from North American
1216 anthropogenic sources, *Atmos. Environ.*, 42, 5193–5204,
1217 <https://doi.org/10.1016/j.atmosenv.2008.02.069>, 2008.

1218 Seo, Y.-S., Han, Y.-J., Choi, H.-D., Holsen, T. M., and Yi, S.-M.: Characteristics of
1219 total mercury (TM) wet deposition: Scavenging of atmospheric mercury species,
1220 *Atmos. Environ.*, 49, 69–76, 10.1016/j.atmosenv.2011.12.031, 2012.

1221 Shen, G., Chen, D., Wu, Y., Liu, L., and Liu, C.: Spatial patterns and estimates of
1222 global forest litterfall, *Ecosphere*, 10, 1–13, 10.1002/ecs2.2587, 2019

1223 Sheu, G.-R., and Lin, N.-H.: Mercury in cloud water collected on Mt. Bamboo in
1224 northern Taiwan during the northeast monsoon season, *Atmos. Environ.*, 45,
1225 4454–4462, 10.1016/j.atmosenv.2011.05.036, 2011.

1226 Sheu, G.-R., and Lin, N.-H.: Characterizations of wet mercury deposition to a remote
1227 islet (Pengjiayu) in the subtropical Northwest Pacific Ocean, *Atmos. Environ.*,
1228 77, 474–481, 10.1016/j.atmosenv.2013.05.038, 2013.

1229 Sheu, G.-R., Gay, D. A., Schmeltz, D., Olson, M., Chang, S.-C., Lin, D.-W., and
1230 Nguyen, L. S. P.: A new monitoring effort for Asia: the Asia Pacific Mercury
1231 Monitoring Network (APMMN), *Atmosphere*, 10(9), 481, 2019.

1232 Siudek, P., Kurzyca, I., and Siepak, J.: Atmospheric deposition of mercury in central
1233 Poland: Sources and seasonal trends, *Atmos. Res.*, 170, 14–22,
1234 10.1016/j.atmosres.2015.11.004, 2016.

1235 Skov, H., Brooks, S. B., Goodsite, M. E., Lindberg, S. E., Meyers, T. P., Landis, M. S.,
1236 Larsen, M. R. B., Jensen, B., McConville, G., and Christensen, J.: Fluxes of
1237 reactive gaseous mercury measured with a newly developed method using
1238 relaxed eddy accumulation, *Atmos. Environ.*, 40, 5452–5463,
1239 <https://doi.org/10.1016/j.atmosenv.2006.04.061>, 2006.

1240 Sommar, J., Zhu, W., Lin, C.-J., and Feng, X.: Field approaches to measure Hg
1241 exchange between natural surfaces and the atmosphere—A review, *Crit. Rev.*
1242 *Environ. Sci. Technol.*, 43, 1657–1739, 10.1080/10643389.2012.671733, 2013a.

1243 Sommar, J., Zhu, W., Shang, L., Feng, X., and Lin, C.-J.: A whole-air relaxed eddy
1244 accumulation measurement system for sampling vertical vapour exchange of
1245 elemental mercury, *Tellus B Chem. Phys. Meteorol.*, 65, 19940,
1246 10.3402/tellusb.v65i0.19940, 2013b.

1247 Sommar, J., Zhu, W., Shang, L., Lin, C.-J., and Feng, X.: Seasonal variations in
1248 metallic mercury (Hg⁰) vapor exchange over biannual wheat–corn rotation
1249 cropland in the North China Plain, *Biogeosciences*, 13, 2029–2049, 10.5194/bg-
1250 13-2029-2016, 2016.

1251 Sprovieri, F., Pirrone, N., Bencardino, M., D'Amore, F., Angot, H., Barbante, C.,
1252 Brunke, E. G., Arcega-Cabrera, F., Cairns, W., Comero, S., Dieguez, M. D.,
1253 Dommergue, A., Ebinghaus, R., Feng, X. B., Fu, X. W., Garcia, P. E., Gawlik, B.
1254 M., Hagestrom, U., Hansson, K., Horvat, M., Kotnik, J., Labuschagne, C.,
1255 Magand, O., Martin, L., Mashyanov, N., Mkololo, T., Munthe, J., Obolkin, V.,
1256 Islas, M. R., Sena, F., Somerset, V., Spandow, P., Varde, M., Walters, C.,
1257 Wangberg, I., Weigelt, A., Yang, X., and Zhang, H.: Five-year records of mercury
1258 wet deposition flux at GMOS sites in the Northern and Southern hemispheres,
1259 *Atmos. Chem. Phys.*, 17, 2689–2708, 10.5194/acp-17-2689-2017, 2017.

1260 Stankwitz, C., Kaste, J. M., and Friedland, A. J.: Threshold increases in soil lead and
1261 mercury from tropospheric deposition across an elevational gradient, *Environ.*
1262 *Sci. Technol.*, 46, 8061–8068, 10.1021/es204208w, 2012.

1263 Streets, D. G., Hao, J. M., Wu, Y., Jiang, J. K., Chan, M., Tian, H. Z., and Feng, X. B.:
1264 Anthropogenic mercury emissions in China, *Atmos. Environ.*, 39, 7789–7806,
1265 <https://doi.org/10.1016/j.atmosenv.2005.08.029>, 2005.

1266 Teixeira, D. C., Montezuma, R. C., Oliveira, R. R., and Silva-Filho, E. V.: Litterfall
1267 mercury deposition in Atlantic forest ecosystem from SE-Brazil, *Environ. Pollut.*,
1268 164, 11–15, 10.1016/j.envpol.2011.10.032, 2012.

1269 Teixeira, D. C., Lacerda, L. D., and Silva-Filho, E. V.: Mercury sequestration by
1270 rainforests: The influence of microclimate and different successional stages,
1271 *Chemosphere*, 168, 1186–1193, 10.1016/j.chemosphere.2016.10.081, 2017.

1272 Torseth, K., Aas, W., Breivik, K., Fjaeraa, A. M., Fiebig, M., Hjellbrekke, A. G.,
1273 Myhre, C. L., Solberg, S., and Yttri, K. E.: Introduction to the European
1274 Monitoring and Evaluation Programme (EMEP) and observed atmospheric
1275 composition change during 1972–2009, *Atmos. Chem. Phys.*, 12, 5447–5481,
1276 10.5194/acp-12-5447-2012, 2012.

1277 Travnikov, O., Angot, H., Artaxo, P., Bencardino, M., Bieser, J., D'Amore, F.,
1278 Dastoor, A., De Simone, F., Diéguez, M. d. C., Dommergue, A., Ebinghaus, R.,
1279 Feng, X. B., Gencarelli, C. N., Hedgecock, I. M., Magand, O., Martin, L.,
1280 Matthias, V., Mashyanov, N., Pirrone, N., Ramachandran, R., Read, K. A.,

1281 Ryjkov, A., Selin, N. E., Sena, F., Song, S. J., Sprovieri, F., Wip, D., Wängberg,
1282 I., and Yang, X.: Multi-model study of mercury dispersion in the atmosphere:
1283 atmospheric processes and model evaluation, *Atmos. Chem. Phys.*, 17, 5271–
1284 5295, 2017.

1285 UN Environment: Global Mercury Assessment 2018, UN Environment Programme,
1286 Chemicals and Health Branch, Geneva, Switzerland, 2019.

1287 Wan, Q., Feng, X., Lu, J., Zheng, W., Song, X., Li, P., Han, S., and Xu, H.:
1288 Atmospheric mercury in Changbai Mountain area, northeastern China II. The
1289 distribution of reactive gaseous mercury and particulate mercury and mercury
1290 deposition fluxes, *Environ. Res.*, 109, 721–727, 10.1016/j.envres.2009.05.006,
1291 2009.

1292 Wang, X., Lin, C. J., and Feng, X.: Sensitivity analysis of an updated bidirectional
1293 air–surface exchange model for elemental mercury vapor, *Atmos. Chem. Phys.*,
1294 14, 6273–6287, 10.5194/acp-14-6273-2014, 2014.

1295 Wang, X., Bao, Z., Lin, C. J., Yuan, W., and Feng, X.: Assessment of global mercury
1296 deposition through litterfall, *Environ. Sci. Technol.*, 50, 8548–8557,
1297 10.1021/acs.est.5b06351, 2016a.

1298 Wang, X., Lin, C.-J., Lu, Z., Zhang, H., Zhang, Y., and Feng, X.: Enhanced
1299 accumulation and storage of mercury on subtropical evergreen forest floor:
1300 Implications on mercury budget in global forest ecosystems, *J. Geophys. Res.*
1301 *Biogeo.*, 121, 2096–2109, 10.1002/2016jg003446, 2016b.

1302 Wang, Z., Zhang, X., Xiao, J., Ci, Z., and Yu, P.: Mercury fluxes and pools in three
1303 subtropical forested catchments, southwest China, *Environ. Pollut.*, 157, 801–
1304 808, 10.1016/j.envpol.2008.11.018, 2009.

1305 Weiss-Penzias, P., Fernandez, D., Moranville, R., and Saltikov, C.: A low cost system
1306 for detecting fog events and triggering an active fog water collector, *Aerosol Air*
1307 *Qual. Res.*, 18, 214–233, 10.4209/aaqr.2016.11.0508, 2018.

1308 Weiss-Penzias, P. S., Gustin, M. S., and Lyman, S. N.: Sources of gaseous oxidized
1309 mercury and mercury dry deposition at two southeastern U.S. sites, *Atmos.*
1310 *Environ.*, 45, 4569–4579, 10.1016/j.atmosenv.2011.05.069, 2011.

1311 Weiss-Penzias, P. S., Gay, D. A., Brigham, M. E., Parsons, M. T., Gustin, M. S., and
1312 Ter Schure, A.: Trends in mercury wet deposition and mercury air concentrations
1313 across the U.S. and Canada, *Sci. Total Environ.*, 568, 546–556,
1314 10.1016/j.scitotenv.2016.01.061, 2016a.

1315 Weiss-Penzias P., Coale K, Heim W, Fernandez D, Oliphant A, Dodge C, Hoskins D,
1316 Farlin J, Moranville R, Olson A. Total- and monomethyl-mercury and major ions
1317 in coastal California fog water: Results from two years of sampling on land and
1318 at sea. *Elem. Sci. Anth.*, 4, 1–18, 10.12952/journal.elementa.000101, 2016b.

1319 Wetang'ula: Preliminary assessment of total mercury in bulk precipitation around
1320 Olkaria Area, Kenya, *Journal of Environmental Science and Engineering*, 1585–
1321 1595, 2011.

1322 Wetherbee, G.A.: Precipitation collector bias and its effects on temporal trends and
1323 spatial variability in National Atmospheric Deposition Program/National Trends
1324 Network data, *Environ. Pollut.*, 223, 90–101, 10.1016/j.envpol.2016.12.036,
1325 2017.

1326 Wetherbee, G.A., and Martin, R.A.: External Quality Assurance Project Report for the
1327 National Atmospheric Deposition Program's National Trends Network and
1328 Mercury Deposition Network, 2015–16. U.S. Geological Survey, Reston,
1329 Virginia, 2018.

1330 Wetherbee, G.A., Latysh, N.E., and Gordon, J.D., and Krabbenhoft, D. P.: Spatial and
1331 temporal variability of the overall error of National Atmospheric Deposition
1332 Program measurements determined by the USGS co-located–sampler program,
1333 water years 1989–2001, *Environ. Pollut.*, 135, 407–418,
1334 10.1016/j.envpol.2004.11.014, 2005.

1335 Wright, G., Gustin, M. S., Weiss-Penzias, P., and Miller, M. B.: Investigation of
1336 mercury deposition and potential sources at six sites from the Pacific Coast to the
1337 Great Basin, USA, *Sci. Total Environ.*, 470–471, 1099–1113,
1338 10.1016/j.scitotenv.2013.10.071, 2014.

1339 Wright, L. P., and Zhang, L.: An approach estimating bidirectional air-surface
1340 exchange for gaseous elemental mercury at AMNet sites, *J. Adv. Model. Earth*
1341 *Sy.*, 7, 35–49, 10.1002/2014ms000367, 2015.

1342 Wright, L. P., Zhang, L. M., and Marsik, F. J.: Overview of mercury dry deposition,
1343 litterfall, and throughfall studies, *Atmos. Chem. Phys.*, 16, 13399–13416,
1344 10.5194/acp-16-13399-2016, 2016.

1345 Xu, L., Chen, J., Yang, L., Yin, L., Yu, J., Qiu, T., and Hong, Y.: Characteristics of
1346 total and methyl mercury in wet deposition in a coastal city, Xiamen, China:
1347 Concentrations, fluxes and influencing factors on Hg distribution in precipitation,
1348 *Atmos. Environ.*, 99, 10–16, 10.1016/j.atmosenv.2014.09.054, 2014.

1349 Yu, Q., Luo, Y., Wang, S. X., Wang, Z. Q., Hao, J. M., and Duan, L.: Gaseous
1350 elemental mercury (GEM) fluxes over canopy of two typical subtropical forests
1351 in south China, *Atmos. Chem. Phys.*, 18, 495–509, 10.5194/acp-18-495-2018,
1352 2018.

1353 Zhang, H. H., Poissant, L., Xu, X. H., and Pilote, M.: Explorative and innovative
1354 dynamic flux bag method development and testing for mercury air-vegetation
1355 gas exchange fluxes, *Atmos. Environ.*, 39, 7481–7493,
1356 doi:10.1016/j.atmosenv.2005.07.068, 2005.

1357 Zhang, L., Brook, J. R., and Vet, R.: A revised parameterization for gaseous dry
1358 deposition in air-quality models, *Atmos. Chem. Phys.*, 3, 2067–2082, DOI
1359 10.5194/acp-3-2067-2003, 2003.

1360 Zhang, L., Blanchard, P., Gay, D. A., Prestbo, E. M., Risch, M. R., Johnson, D.,
1361 Narayan, J., Zsolway, R., Holsen, T. M., Miller, E. K., Castro, M. S., Graydon, J.
1362 A., St Louis, V. L., and Dalziel, J.: Estimation of speciated and total mercury dry
1363 deposition at monitoring locations in eastern and central North America, *Atmos.*
1364 *Chem. Phys.*, 12, 4327–4340, 10.5194/acp-12-4327-2012, 2012.

1365 Zhang, L., and He, Z.: Technical Note: An empirical algorithm estimating dry
1366 deposition velocity of fine, coarse and giant particles, *Atmos. Chem. Phys.*, 14,
1367 3729–3737, 10.5194/acp-14-3729-2014, 2014.

1368 Zhang, L., Wang, S. X., Wu, Q. R., Wang, F. Y., Lin, C.-J., Zhang, L. M., Hui, M. L.,
1369 Yang, M., Su, H. T., and Hao, J. M.: Mercury transformation and speciation in
1370 flue gases from anthropogenic emission sources: a critical review, *Atmos. Chem.*
1371 *Phys.*, 16, 2417–2433, 10.5194/acp-16-2417-2016, 2016a.

1372 Zhang, L., Wu, Z., Cheng, I., Wright, L. P., Olson, M. L., Gay, D. A., Risch, M. R.,
1373 Brooks, S., Castro, M. S., Conley, G. D., Edgerton, E. S., Holsen, T. M., Luke,
1374 W., Tordon, R., and Weiss-Penzias, P.: The estimated six-year mercury dry
1375 deposition across North America, *Environ. Sci. Technol.*, 50, 12864–12873,
1376 10.1021/acs.est.6b04276, 2016b.

1377 Zhang, L. M., Gong, S. L., Padro, J., and Barrie, L.: A size-segregated particle dry
1378 deposition scheme for an atmospheric aerosol module, *Atmos. Environ.*, 35, 549–
1379 560, Doi 10.1016/S1352-2310(00)00326-5, 2001.

1380 Zhang, L. M., Moran, M. D., Makar, P. A., Brook, J. R., and Gong, S. L.: Modelling
1381 gaseous dry deposition in AURAMS: A unified regional air-quality modelling
1382 system, *Atmos. Environ.*, 36, 537–560, Doi 10.1016/S1352-2310(01)00447-2,

1383 2002.

1384 Zhang, L. M., Wright, L. P., and Blanchard, P.: A review of current knowledge
1385 concerning dry deposition of atmospheric mercury, *Atmos. Environ.*, 43, 5853–
1386 5864, 10.1016/j.atmosenv.2009.08.019, 2009.

1387 Zhang, L., Wang, S. X., Wang, L., and Hao, J. M.: Atmospheric mercury
1388 concentration and chemical speciation at a rural site in Beijing, China:
1389 implications of mercury emission sources, *Atmos. Chem. Phys.*, 13, 10505–
1390 10516, <https://doi.org/10.5194/acp-13-10505-2013>, 2013.

1391 Zhang, Y., Jaeglé, L., van Donkelaar, A., Martin, R. V., Holmes, C. D., Amos, H. M.,
1392 Wang, Q., Talbot, R., Artz, R., Brooks, S., Luke, W., Holsen, T. M., Felton, D.,
1393 Miller, E. K., Perry, K. D., Schmeltz, D., Steffen, A., Tordon, R., Weiss-Penzias,
1394 P., and Zsolway, R.: Nested-grid simulation of mercury over North America,
1395 *Atmos. Chem. Phys.*, 12, 6095–6111, doi:10.5194/acp-12-6095-2012, 2012.

1396 Zhang, Y., Liu, R., Wang, Y., Cui, X., and Qi, J.: Change characteristic of atmospheric
1397 particulate mercury during dust weather of spring in Qingdao, China, *Atmos.*
1398 *Environ.*, 102, 376–383, 10.1016/j.atmosenv.2014.12.005, 2015.

1399 Zhang, Y., Jacob, D. J., Horowitz, H. M., Chen, L., Amos, H. M., Krabbenhoft, D. P.,
1400 Slemr, F., St Louis, V. L., and Sunderland, E. M.: Observed decrease in
1401 atmospheric mercury explained by global decline in anthropogenic emissions,
1402 *Proc. Natl. Acad. Sci. U.S.A.*, 113(3), 526–531, 2016.

1403 Zhao, Z., Wang, D., Wang, Y., Mu, Z., and Zhu, J.: Wet deposition flux and runoff
1404 output flux of mercury in a typical small agricultural watershed in Three Gorges
1405 Reservoir areas, *Environ. Sci. Pollut. Res. Int.*, 22, 5538–5551, 10.1007/s11356-
1406 014-3701-2, 2015.

1407 Zhao, L.S., Xu, L.L., Wu, X., Zhao, G.Q., Jiao, L., Chen, J.S., Hong Y.W., Deng J.J.,
1408 Chen, Y.T., Yang, K., Hu, G.R., Yu, R.L.: Characteristics and sources of mercury
1409 in precipitation collected at the urban, suburban and rural sites in a city of
1410 Southeast China, *Atmos. Res.*, 211, 21–29, 10.1016/j.atmosres.2018.04.019,
1411 2018.

1412 Zhou, J., Wang, Z., Sun, T., Zhang, H., and Zhang, X.: Mercury in terrestrial forested
1413 systems with highly elevated mercury deposition in southwestern China: The risk
1414 to insects and potential release from wildfires, *Environ. Pollut.*, 212, 188–196,
1415 10.1016/j.envpol.2016.01.003, 2016.

1416 Zhou, J., Wang, Z., Zhang, X., and Gao, Y.: Mercury concentrations and pools in four

1417 adjacent coniferous and deciduous upland forests in Beijing, China, *J. Geophys.*
1418 *Res. Biogeo.*, 122, 1260–1274, 10.1002/2017jg003776, 2017.

1419 Zhu, J., Wang, T., Talbot, R., Mao, H., Yang, X., Fu, C., Sun, J., Zhuang, B., Li, S.,
1420 Han, Y., and Xie, M.: Characteristics of atmospheric mercury deposition and
1421 size-fractionated particulate mercury in urban Nanjing, China, *Atmos. Chem.*
1422 *Phys.*, 14, 2233–2244, 10.5194/acp-14-2233-2014, 2014.

1423 Zhu, J., Wang, T., Bieser, J., and Matthias, V.: Source attribution and process analysis
1424 for atmospheric mercury in eastern China simulated by CMAQ-Hg, *Atmos.*
1425 *Chem. Phys.*, 15, 8767–8779, <https://doi.org/10.5194/acp-15-8767-2015>, 2015.

1426 Zhu, W., Sommar, J., Lin, C. J., and Feng, X.: Mercury vapor air–surface exchange
1427 measured by collocated micrometeorological and enclosure methods – Part I:
1428 Data comparability and method characteristics, *Atmos. Chem. Phys.*, 15, 685–
1429 702, 10.5194/acp-15-685-2015, 2015b.

1430 Zhu, W., Lin, C.-J., Wang, X., Sommar, J., Fu, X., and Feng, X.: Global observations
1431 and modeling of atmosphere–surface exchange of elemental mercury: A critical
1432 review, *Atmos. Chem. Phys.*, 16, 4451–4480, 10.5194/acp-16-4451-2016, 2016.

1433

1434 **Table Captions**

1435 **Table 1.** Summary of relative uncertainties of different types of Hg deposition to
1436 terrestrial surfaces.

1437

1438 **Table 1.** Summary of relative uncertainties of different types of Hg deposition to
 1439 terrestrial surfaces.

Type of Hg deposition	Relative uncertainty in observation (%)	Relative uncertainty in simulation (%)
Wet deposition	±(20–35)	±(30–55)
Precipitation	±(15–20)	±(30–50)
Cloud, fog, dew, and frost	±(200–300)	±(200–300)
Dry deposition	±(50–90)	±(90–130)
GOM dry deposition	±(60–70)	±(150–300)
PBM dry deposition	±(80–100)	±(120–150)
GEM dry deposition	±(100–200)	±(100–400)
Forest deposition	±(15–25)	±(40–70)
Litterfall	±(20–30)	±(60–100)
Throughfall	±(20–30)	±(50–90)
Overall	±(25–50)	±(45–70)

1440

1441

1442 **Figure Captions**

1443 **Figure 1.** Global distribution of the observed Hg wet deposition fluxes by observation
1444 networks around the world ($\mu\text{g m}^{-2} \text{yr}^{-1}$).

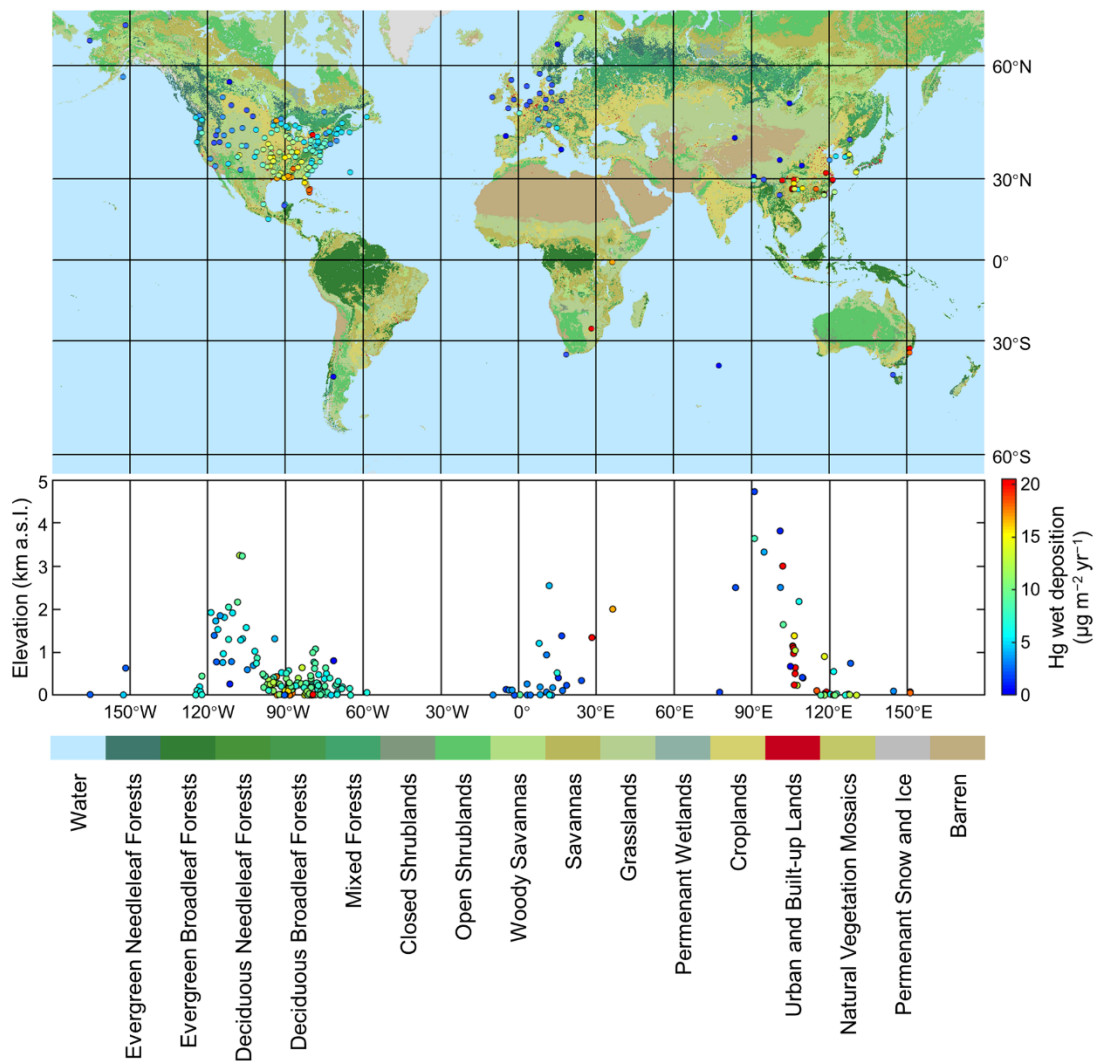
1445 **Figure 2.** Global distribution of the (a) GOM, (b) PBM, and (c) GEM dry deposition
1446 fluxes ($\mu\text{g m}^{-2} \text{yr}^{-1}$) from observation-based estimation.

1447 **Figure 3.** Relationship between the elevation and the GOM dry deposition flux.

1448 **Figure 4.** Comparison between the GOM dry deposition fluxes from direct
1449 observations and from model simulations based on measurements of GOM
1450 concentrations. The numbers in brackets stand for the numbers of samples.

1451 **Figure 5.** Dry deposition fluxes (cyan columns with black bars as standard deviations)
1452 of (a) GOM, (b) PBM and (c) GEM for different terrestrial surface types. “Water”
1453 stands for the terrestrial surfaces near water. The numbers in brackets stand for the
1454 numbers of samples.

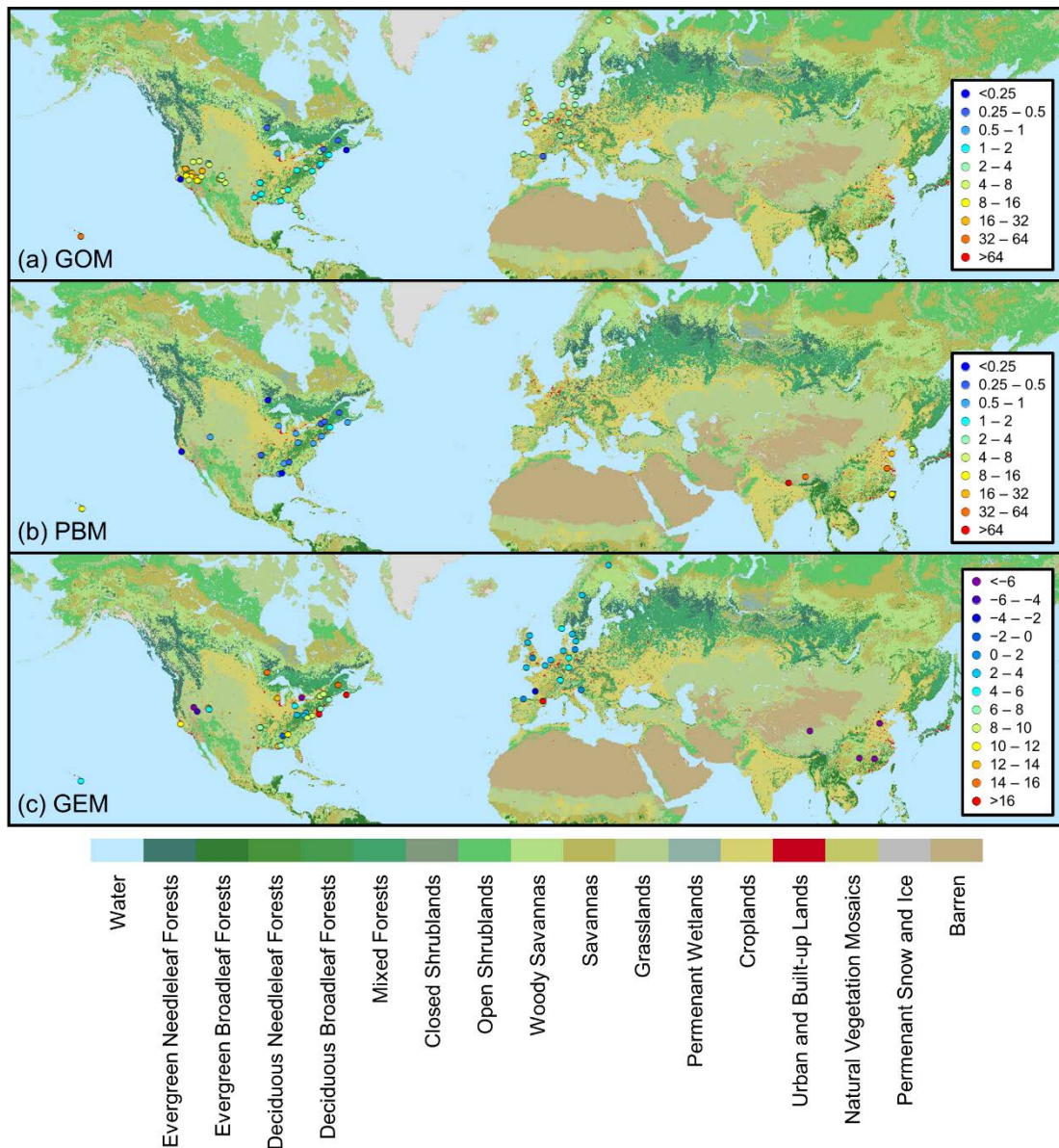
1455



1456

1457 **Figure 1.** Global distribution of the observed Hg wet deposition fluxes by observation
 1458 networks around the world ($\mu\text{g m}^{-2} \text{yr}^{-1}$).

1459

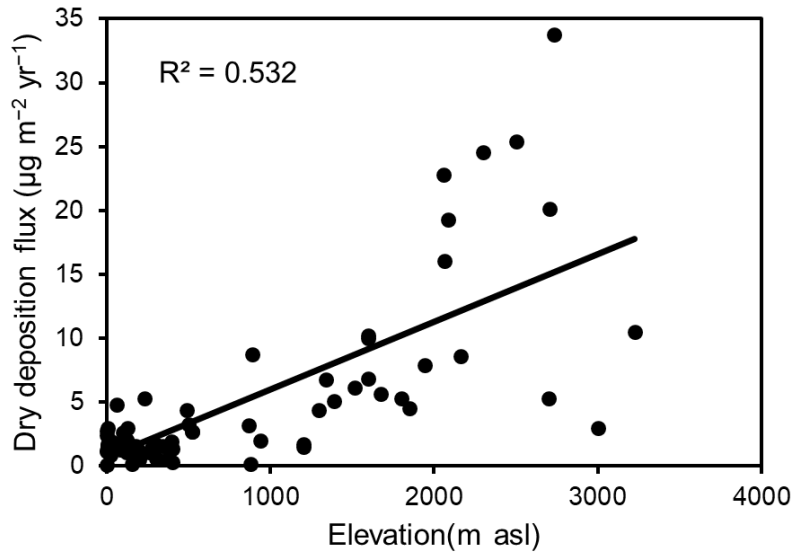


1460

1461 **Figure 2.** Global distribution of the (a) GOM, (b) PBM, and (c) GEM dry deposition

1462 fluxes ($\mu\text{g m}^{-2} \text{yr}^{-1}$) from observation-based estimation.

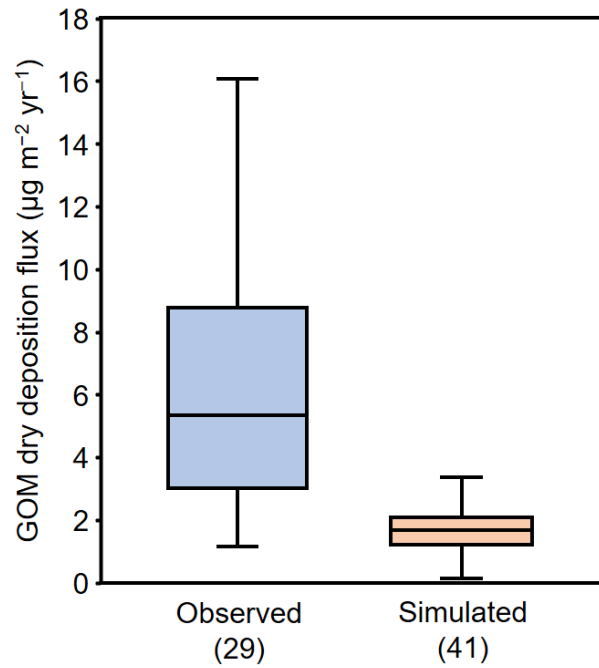
1463



1464

1465 **Figure 3.** Relationship between the elevation and the GOM dry deposition flux.

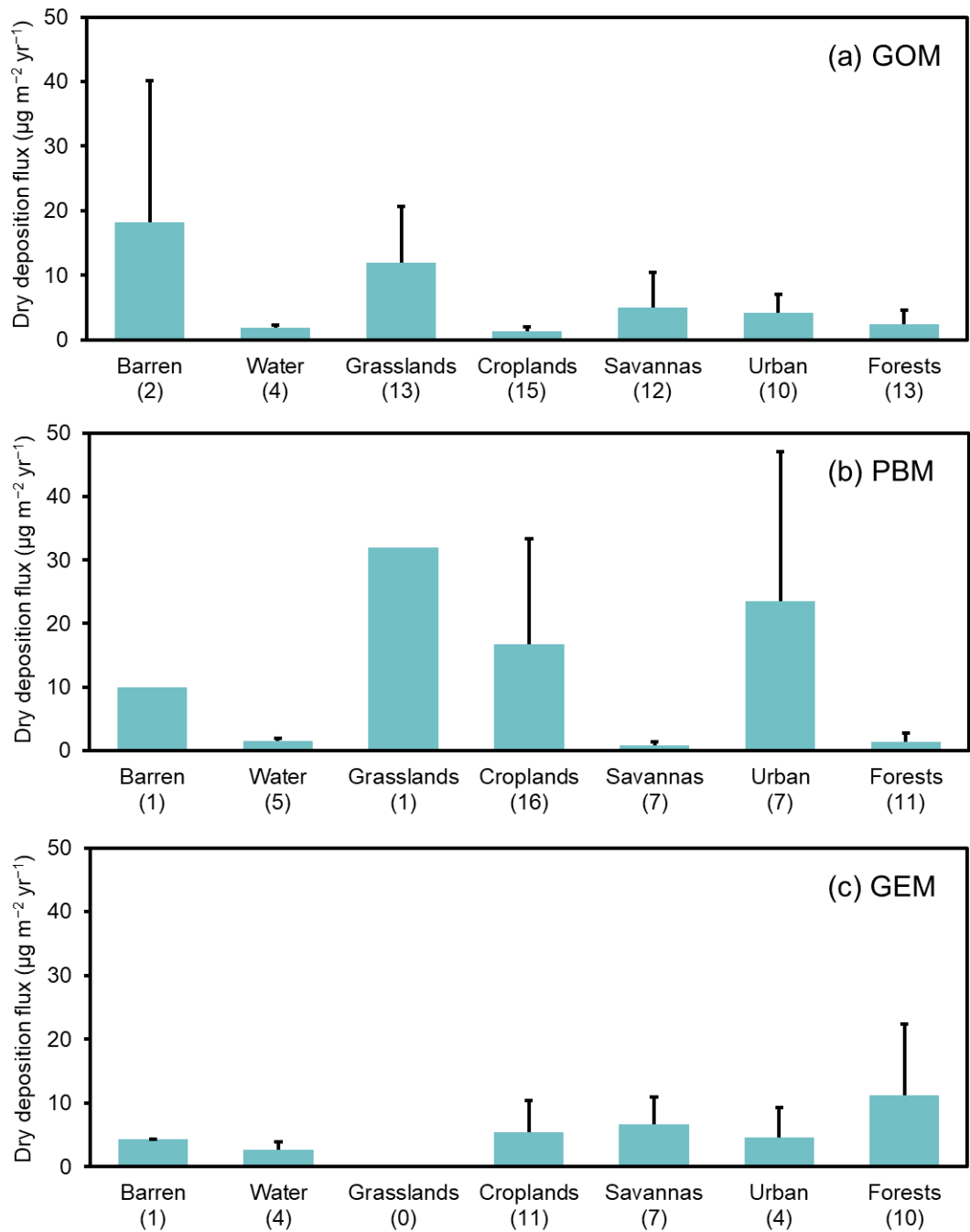
1466



1467

1468 **Figure 4.** Comparison between the GOM dry deposition fluxes from direct
1469 observations and from model simulations based on measurements of GOM
1470 concentrations. The numbers in brackets stand for the numbers of samples.

1471



1472

1473 **Figure 5.** Dry deposition fluxes (cyan columns with black bars as standard deviations)

1474 of (a) GOM, (b) PBM and (c) GEM for different terrestrial surface types. “Water”

1475 stands for the terrestrial surfaces near water. The numbers in brackets stand for the

1476 numbers of samples.

1477